Robust Hybrid Supervisory Control for Spacecraft Close Proximity Missions

Bharani P. Malladi[a,1,*], Ricardo G. Sanfelice[b,2], Eric A. Butcher[a,1]

[a] *Department of Aerospace and Mechanical Engineering, University of Arizona, 1130 N Mountain Ave, 85721, Tucson, AZ, USA*
[b] *Department of Computer Engineering, University of California at Santa Cruz, 1156 High Street MS:SOE3, 95064, Santa Cruz, CA, USA*

Abstract

We consider the problem of rendezvous, proximity operations, and docking of an autonomous spacecraft. The problem can be conveniently divided into three phases: 1) rendezvous phase; 2) docking phase; and 3) docked phase. On each phase the task to perform is different, and requires a different control algorithm. Angle and range measurements are available for the entire mission, but constraints and tasks to perform are different depending on the phase. Due to the different constraints, available measurements, and tasks to perform on each phase, we study this problem using a hybrid systems approach, in which the system has different modes of operation for which a suitable controller is to be designed. Following this approach, we characterize the family of individual controllers and the required properties they should induce to the closed-loop system to solve the problem within each phase of operation. Furthermore, we propose a supervisory algorithm that robustly coordinates the individual controllers so as to provide a solution to the problem. In addition, we present specific controller designs that appropriately solve the control problems for individual phases and validate them numerically.

[*] Corresponding author

URL: malladi@email.arizona.edu (Bharani P. Malladi), ricardo@ucsc.edu (Ricardo G. Sanfelice), ebutcher@email.arizona.edu (Eric A. Butcher)

[1] Research by B. P. Malladi, E. A. Butcher is partially supported by Dynamics, Control, and Systems Diagnostics Program of NSF Grants no. CMMI-1561836.

[2] Research by R. G. Sanfelice has been partially supported by the National Science Foundation under Grant no. ECS-1710621, Grant no. CNS-1544396, and Grant no. CNS-2039054, by the Air Force Office of Scientific Research under Grant no. FA9550-16-1-0015, Grant no. FA9550-19-1-0053, Grant no. FA9550-19-1-0169, and Grant no. FA9550-20-1-0238, and by the Army Research Office under Grant no. W911NF-20-1-0253, and by CITRIS and the Banatao Institute at the University of California.

1. Introduction

1.1. Background, Motivation, and Problem Statement

Recent developments in the field of automation and control have motivated the use of new approaches and strategies for control and navigation in advanced space missions; see [1] and the references in[3]. These space missions include spacecraft rendezvous, proximity operations and docking [2, 3, 4, 5, 6, 7], orbital debris removal [8, 9], and rendezvous to non-cooperative free-flying space objects [10, 11] to name a few. Such advanced space missions present several challenges and may require switching between multiple strategies to achieve robust performance. In most practical applications, the data required to design such advanced switching strategies may be affected by environmental perturbations. Hence, the work in this paper focuses on the study of robust control applied to spacecraft close-proximity missions.

Rendezvous and docking play a crucial role in space missions that are not only critical phases in routine manned spaceflight (e.g., Apollo, Space Shuttle, International Space Station (ISS)) but also in more advanced operations, some of which demanding autonomous solutions, such as resupply (e.g., Automated Transfer Vehicle (ATV), H-II Transfer Vehicle (HTV), Cygnus, Dragon to ISS), assembly (e.g., ISS, proposed large-aperture telescopes, large space structures/habitats), servicing/repair (e.g., Hubble, DARPA Phoenix), refueling (e.g., Orbital Express, proposed fuel depots) rendezvous and docking is useful. The relative motion between two or more spacecraft in close proximity are often modeled assuming a circular chief orbit and a deputy orbit linearized about the chief's position. This results in the well-known Clohessy-Wiltshire-Hill (CWH) equations [12, 13]. In most cases the target spacecraft is passive while the chaser spacecraft is controlling the rendezvous and docking. The Concept of Operations (CONOPS) of the space missions mentioned above share the following phases (see [1]):

1. Rendezvous phase: it describes one spacecraft approaching another within 10km to 100m as Figure 1 shows;

2. Docking phase: it describes final maneuvers executed to engage docking ports within 100 to 0m as Figure 1 shows;

3. Docked phase: it describes the control of the rigidly attached spacecraft pair as Figure 2 shows.

Closed-loop feedback control solutions for spacecraft relative motion for close-proximity missions include LQR control [14], time-varying gain control [15], and output tracking schemes that successfully reject disturbances [16]. In [17] a rendezvous and docking problem along with obstacle avoidance and plume

[3]An invited session on the topic of 'A Spacecraft Benchmark Problem for Analysis & Control of Hybrid Systems' organized at the 2016 IEEE 55th Conference on Decision and Control (CDC)

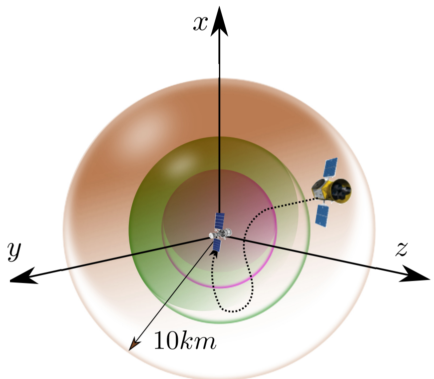

(a) Rendezvous phase

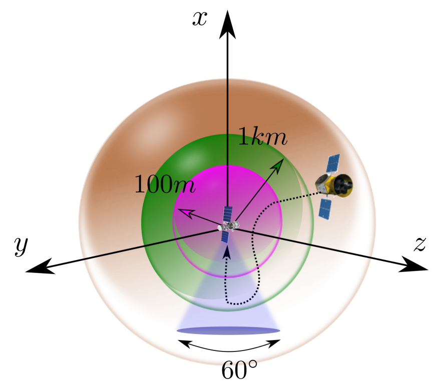

(b) Docking phase

Figure 1: Rendezvous and docking phase between the chaser and target spacecraft.

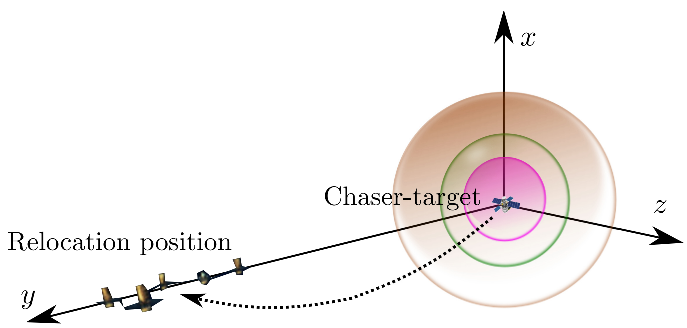

Figure 2: Docked phase between chaser and target spacecraft.

impingement is solved using an online-and-offline optimal control technique. In this method, an optimal control algorithm with probabilistic search is used to generate a series of control actions off-line and a method based on the gradient descent formulation is used to achieve real-time obstacle avoidance. Model predictive control (MPC) strategies for rendezvous and docking missions are suggested in [18, 19, 20] and an MPC algorithm for rotating/tumbling platform with obstacle avoidance is presented in [21, 22]. A detailed discussion on the current state of model predictive control approaches to various aerospace systems is presented in [23]. In [24], a two-stage optimal control strategy is implemented. This controller includes equations of motion that are differentially flat in relative coordinates in the first stage and an MPC with linearized dynamics in second stage. Formal verification algorithms are applied to spacecraft rendezvous problem in [25, 26] with simulation-driven reachability analysis using the verification tool DryVR [27]. In addition, safe reachable sets for the above mentioned spacecraft rendezvous problem with minimum fuel and minimum time trajectories are discussed in [28].

In certain control applications, control design tools that divide the problem into subproblems for which several control laws can be designed independently and then combined to solve the original problem are prevalent for many reasons. They reduce design and implementation time as well as add modularity and flexibility to the control system. They are also appropriate when a single, continuous stabilizing control law does not exist or when its design is not straightforward. Moreover, multiple control laws, when properly designed and applied to the plant, can enhance the robustness properties of the closed-loop system. Such a “divide and conquer” approach to control design is also ubiquitous in control problems where precise control is desired nearby particular operating points while less stringent conditions need to be satisfied at other points. This corresponds to the problem of uniting local and global controllers in which two control laws are used: one that works only locally (perhaps guaranteeing good performance) and another that is capable of steering the system trajectories to a neighborhood of the operating point where the local control law works [29, 30]. This patchy feedback control strategy, which consists of partitioning the state space into disjoint regions in which a state-feedback law is designed in such a way that the desired point or set is globally asymptotically stabilized, is presented in [31, 32]. The related throw-and-catch approach is discussed in [33], which extends the uniting approach described above by including open-loop control laws. As argued above, these capabilities are highly desired for CONOPS due to varied mission requirements, and in this work we extend and apply such “divide and conquer” approach to spacecraft close-proximity missions.

The concepts of hybrid system theory (see [34, 35]) that include both continuous and discrete dynamics have shown potential to address the issues of chattering with limited sensor/actuator data. These hybrid system techniques formulate a hysteresis (overlap) region to switch between various controllers thus overcoming the issue of chattering.

1.2. Contributions

In this paper, we apply the divide-and-conquer approach enabled by hybrid feedback control to the problem of rendezvous, proximity operations, and docking of an autonomous spacecraft modeled using the CWH equations, which are widely used in the literature of spacecraft control. This problem consists of the following three main phases:

1. Rendezvous phase with range and angle measurements, as Figure 1 shows;

2. Docking phase with range and angle measurements, as Figure 1 shows;

3. Docked phase with range and angle measurements, as Figure 2 shows.

The state constraints, available measurements, as well as the tasks to perform are different for each of the phases. This change in the specifications and in the function defining the measurements lead to a nonsmooth dynamical system.

Due to the interest in a feedback controller that does not exhibit chattering, that can be designed in a modular fashion and systematically, and that guarantees robust stability properties, we propose a hybrid systems approach, in which the system has different modes of operation, and design both the individual controllers for each mode as well as the algorithm that supervises them. More precisely, we contribute to the problem of rendezvous, proximity operations, and docking of an autonomous spacecraft by

- Formulating the problem to be solved based on measurements available, and tasks to be performed in each of the rendezvous, docking and docked phases (see Section 2).
- Characterizing the family of individual controllers and the required properties they should induce to the closed-loop system to solve the problem within each phase of operation (see Section 4).
- Providing specific controller designs that appropriately solve the control problems for individual phases (see Sections 5).
- Designing a supervisor that robustly coordinates the individual controllers so as to provide a solution to the problem (see Sections 6).
- Results simulating and validating the above mentioned steps numerically is presented in Section 7.

2. Preliminaries

2.1. Notation

The following notation and definitions are used throughout the paper. An n-dimensional Euclidean space is denoted by $\mathbb{R}^n$. The set of real numbers are denoted by $\mathbb{R}$, $\mathbb{Z}$ denotes the integers and $\mathbb{R}_{\geq 0}$ denotes the nonnegative real numbers, i.e., $\mathbb{R}_{\geq 0} = [0, \infty)$. The natural numbers including 0, i.e., $\mathbb{N} = \{0, 1, \ldots\}$ are denoted by $\mathbb{N}$. The set of positive semidefinite and positive definite, symmetric matrices, respectively, are denoted by $\Pi_{\geq 0}$ and $\Pi_{>0}$. An open unit ball in a Euclidean space is denoted by $\mathbb{B}$. Given a set $\mathcal{A} \subset \mathbb{R}^n$ and a point $x \in \mathbb{R}^n$, $|x|_{\mathcal{A}} := \inf_{y \in \mathcal{A}} |x - y|$. The equivalent notation $[x^\top \; y^\top]^\top$ and (x, y) is used for vectors. Given a vector $y \in \mathbb{R}^n$, $|y|$ denotes its Euclidean norm. For a generic vector norm $|.|$, its corresponding induced matrix norm on P is given by $|P|$. Given a symmetric positive matrix P, $\lambda(P)$ denotes its eigenvalue. An identity matrix of appropriate dimension is denoted by I and I_s denotes the identity matrix with dimension $s \times s$. An $n \times p$ zero vector/matrix is represented by $\mathbf{0}_{n \times p}$. A function $\alpha : \mathbb{R}_{\geq 0} \to \mathbb{R}_{\geq 0}$ is said to belong to class-$\mathcal{K}$ if it is continuous, zero at zero, and strictly increasing. A function $\alpha : \mathbb{R}_{\geq 0} \to \mathbb{R}_{\geq 0}$ is said to belong to class-$\mathcal{K}_\infty$ if it belongs to class-$\mathcal{K}$ and is unbounded. A function $\beta : \mathbb{R}_{\geq 0} \times \mathbb{R}_{\geq 0} \to \mathbb{R}_{\geq 0}$ is said to belong to class-$\mathcal{KL}$ if it is nondecreasing in its first argument, nonincreasing in its second argument, and $\lim_{s \searrow 0} \beta(s, t) = \lim_{t \to \infty} \beta(s, t) = 0$.

2.2. Spacecraft relative motion

In this paper, we consider a model of the chaser spacecraft given by the so-called Clohessy-Wiltshire-Hill (CWH) equations, namely,

$$\begin{aligned} \ddot{x} - 2n\dot{y} - 3n^2 x &= \tfrac{F_x}{m_c}, \\ \ddot{y} + 2n\dot{x} &= \tfrac{F_y}{m_c}, \\ \ddot{z} + n^2 z &= \tfrac{F_z}{m_c}, \end{aligned} \tag{1}$$

where (x, y, z) and $(\dot{x}, \dot{y}, \dot{z})$ are the position and velocity, in the rotating Hill frame whose origin is at the location of the target spacecraft and whose x, y, and z directions point in the local radial, along-track, and cross-track directions, respectively. The control forces in the x, y and z directions, respectively, are F_x, F_y and F_z, the mass of the chaser is m_c, and $n := \sqrt{\frac{\mu}{{r_o}^3}}$ is the orbital mean motion of the target, where μ is the gravitational parameter of the Earth and r_o is the orbit radius of the target spacecraft. The state space representation of (1) is given by

$$\dot{\eta} = A\eta + Bu, \tag{2}$$

where $\eta := (x, y, z, \dot{x}, \dot{y}, \dot{z}) \in \mathbb{R}^6$ is the state vector, $u := (F_x, F_y, F_z) \in \mathbb{R}^3$ is the input vector, and

$$A := \begin{bmatrix} 0 & 0 & 0 & 1 & 0 & 0 \\ 0 & 0 & 0 & 0 & 1 & 0 \\ 0 & 0 & 0 & 0 & 0 & 1 \\ 3n^2 & 0 & 0 & 0 & 2n & 0 \\ 0 & 0 & 0 & -2n & 0 & 0 \\ 0 & 0 & -n^2 & 0 & 0 & 0 \end{bmatrix}, B := \begin{bmatrix} 0 & 0 & 0 \\ 0 & 0 & 0 \\ 0 & 0 & 0 \\ \frac{1}{m_c} & 0 & 0 \\ 0 & \frac{1}{m_c} & 0 \\ 0 & 0 & \frac{1}{m_c} \end{bmatrix}$$

are the state and input matrices, respectively. In the sections to follow, we will define the measurements and constraints based on the region of operation of the system.

2.3. Well-posed hybrid systems

To overcome topological issues with antipodal points as mentioned in Section 1.1, in this paper, we formulate the problem of rigid body pose control in the framework for hybrid systems as in [35, 34]. Hybrid systems are dynamical systems with both continuous and discrete dynamics. A hybrid system $\mathcal{H} = (C, F, D, G)$ is defined by the following objects:

- A set $C \subset \mathbb{R}^n$ called the *flow set*;
- A map $F : \mathbb{R}^n \rightrightarrows \mathbb{R}^n$ called the *flow map*;
- A set $D \subset \mathbb{R}^n$ called the *jump set*;
- A map $G : \mathbb{R}^n \rightrightarrows \mathbb{R}^n$ called the *jump map*.

The flow map F defines the continuous dynamics on the flow set C, while the jump map G defines the discrete dynamics on the jump set D. In addition, $C \subset \operatorname{dom} F$, $D \subset \operatorname{dom} G$, such that F and G are nonempty on C and D, respectively. These objects are referred to as the data of the hybrid system $\mathcal{H}$. Denoting the state of the hybrid system $\mathcal{H}$ by χ, the notation χ^+ indicates the values of the state after the jump. A solution ϕ to $\mathcal{H}$ is given on an extended time domain, called *hybrid time domain*, that is parametrized by the pairs (t, j), where t is the ordinary time component and j is a discrete parameter that keeps track of the number of jumps; see [35, Definition 2.6]. Given a solution ϕ to $\mathcal{H}$, the notation $\operatorname{dom} \phi$ represents its domain, which is a hybrid time domain. A solution to $\mathcal{H}$ is said to be *nontrivial* if $\operatorname{dom} \phi$ contains at least one point different from $\{(0,0)\}$, *complete* if $\operatorname{dom} \phi$ is unbounded, and *maximal* if it cannot be extended, i.e., it is not a truncated version of another solution. The set $\mathcal{S}_{\mathcal{H}}(\xi)$ denotes the set of all maximal solutions to $\mathcal{H}$ from ξ. This framework also permits explicit modeling of perturbations in the system dynamics, a feature that is very useful for robust stability analysis of dynamical systems; see [35] for more details.

2.4. Stability theory

In this paper, we employ the following asymptotic stability notion for the closed-loop hybrid systems.

Definition 2.1 ((pre-)asymptotic stability [35, Definition 3.6]). *Consider a hybrid system $\mathcal{H}$. A closed set $\mathcal{A} \subset \mathbb{R}^n$ is said to be*

- stable *for $\mathcal{H}$ if for each $\varepsilon > 0$ there exists $\delta > 0$ such that any solution ϕ to $\mathcal{H}$ with $|\phi(0,0)|_{\mathcal{A}} \leq \delta$ satisfies $|\phi(t,j)|_{\mathcal{A}} \leq \varepsilon$ for all $(t,j) \in \operatorname{dom} \phi$;*

- pre-attractive *for $\mathcal{H}$ if there exists $\delta > 0$ such that any solution ϕ to $\mathcal{H}$ with $|\phi(0,0)|_{\mathcal{A}} \leq \delta$ is bounded and if it is complete then $\phi(t,j) \to \mathcal{A}$ as $t + j \to \infty$;*

- pre-asymptotically stable *if it is both pre-stable and pre-attractive;*

- asymptotically stable *if it is pre-asymptotically stable and there exists $\delta > 0$ such that any maximal solution ϕ to $\mathcal{H}$ with $|\phi(0,0)|_{\mathcal{A}} \leq \delta$ is complete.*

The set of all points in $C \cup D$ from which all solutions are bounded and the complete ones converge to $\mathcal{A}$ is called the basin of pre-attraction[4] *of $\mathcal{A}$. When the basin of (pre-)attraction is equal to $\mathbb{R}^n$, the set $\mathcal{A}$ is said to be* globally (pre-)asymptotically stable. △

[4]Note that by definition, the basin of pre-attraction contains a neighborhood of $\mathcal{A}$. In addition, points in $\mathbb{R}^n \setminus (C \cup D)$ always belong to the basin of pre-attraction since there are no solutions starting at such points, and therefore, there is nothing to be checked. Furthermore, if $\mathcal{A}$ is pre-asymptotically stable and every maximal solution is complete, then we say that $\mathcal{A}$ is asymptotically stable (without the prefix "pre").

Additional details on hybrid system theory can be found in [35, 36]. With these preliminaries on the hybrid system theory, next we present the problem formulation.

3. Problem Formulation

With this general overview, in this paper, we solve the problem of CONOPS of a space mission consisting of rendezvous, docking, docked phase described in Section 1.1. Let us consider the Clohessy-Wiltshire-Hill (CWH) equations as given in (1). For this model, let us consider that the relative position between the chaser and the target is represented by $\rho(x, y, z) := \sqrt{x^2 + y^2 + z^2}$. Let $\mathcal{N}^n(0, \sigma^2)$ be the set of measurable functions in an n-dimensional Euclidean space with Gaussian distribution having zero mean and variance σ^2. We are ready to state the problem to solve (see [1]) as follows.

Problem 1: Given positive constants m_c, m_t, μ, r_o, $u_{\max}$, $\rho_{\max} > \rho_r > \rho_d$, $\overline{V}, V_{\max}$, σ_1, σ_2, σ_3, σ_4, $t_f > t_e$, for some $t_{2f} < t_{3f} < t_{4f}$ such that $t_{3f} \leq t_e$, $t_{4f} \leq t_f$, $\theta \in [0, \frac{\pi}{2})$, and $(x_p, y_p, z_p) \in \mathbb{R}^3$, design a feedback controller that measures angle and range

$$\begin{aligned} y &= h(\eta) + v, \\ h(\eta) &= \left(\arctan\left(\tfrac{y}{x}\right), \arcsin\left(\tfrac{z}{\rho(x,y,z)}\right), \rho(x, y, z)\right), \end{aligned} \tag{3}$$

where $\arctan : \mathbb{R} \to [-\pi, \pi]$, $\arcsin : \mathbb{R} \to [0, 2\pi]$ are four-quadrant inverse tangent and inverse sin, respectively, $v \in \mathcal{N}^n(0, \sigma_n^2)$, $n \in \{1, 2, 3, 4\}$; and assigns $u \in \mathbb{R}^3$ such that for every initial condition

$$\eta_0 \in \mathcal{M}_0 := \left\{\eta \in \mathbb{R}^6 : \ \rho(x, y, z) \in [0, \rho_{\max}], \rho(\dot{x}, \dot{y}, \dot{z}) \in [0, \overline{V}]\right\}$$

of the chaser with dynamics as in (2) such that the following conditions are satisfied:

a) Input constraints: The control signal $t \mapsto u(t)$ satisfies the "maximum thrust" constraint $\sup_{t \geq 0} \max\{|F_x(t)|, |F_y(t)|, |F_z(t)|\} \leq u_{\max}$ namely, for each $t \geq 0$,

$$u(t) \in \mathcal{U}_P := \left\{u \in \mathbb{R}^3 : \max\{|F_x|, |F_y|, |F_z|\} \leq u_{\max}\right\}; \tag{4}$$

b) Phase I constraints: As shown in Figure 3, for each

$$\eta \in \mathcal{M}_1 := \left\{\eta \in \mathbb{R}^6 \ : \ \rho(x, y, z) \in [\rho_r, \infty) \ \right\},$$

angle and range measurements $y \in \mathbb{R}^3$ are available as in (3), namely,

$$h(\eta) = \left(\arctan\left(\frac{y}{x}\right), \arcsin\left(\frac{z}{\rho(x, y, z)}\right), \rho(x, y, z)\right) \tag{5}$$

and $v \in \mathcal{N}^3(0, \sigma_1^2)$;

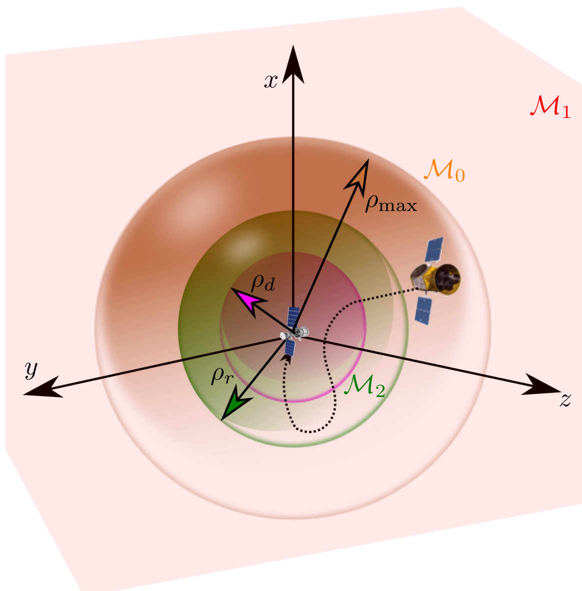

Figure 3: Constrains defining Phase I and Phase II.

c) Phase II constraints: As shown in Figure 3, for each

$$\eta \in \mathcal{M}_2 := \left\{ \eta \in \mathbb{R}^6 \; : \; \rho(x,y,z) \in [\rho_d, \rho_r) \right\}, \tag{6}$$

angle and range measurements $y \in \mathbb{R}^3$ are available as in (3), that is, we have h as in (5) and $v \in \mathcal{N}^2(0, \sigma_2^2)$;

d) Phase III constraints: As shown in Figure 4, for each

$$\eta \in \mathcal{M}_3^a := \left\{ \eta \in \mathbb{R}^6 \; : \; \rho(x,y,z) \in [0, \rho_d) \right\},$$

$y \in \mathbb{R}^3$ is available as in (3) and $v \in \mathcal{N}^2(0, \sigma_3^2)$.
While, in addition, if $\eta \in \mathcal{M}_3^a \cap \mathcal{M}_3^b$, where

$$\mathcal{M}_3^b(\theta) := \left\{ \eta \in \mathbb{R}^6 : \begin{bmatrix} \sin(\theta/2) & \cos(\theta/2) & 0 \\ \sin(\theta/2) & -\cos(\theta/2) & 0 \\ \sin(\theta/2) & 0 & \cos(\theta/2) \\ \sin(\theta/2) & 0 & -\cos(\theta/2) \end{bmatrix} \begin{bmatrix} x \\ y \\ z \end{bmatrix} \leq \begin{bmatrix} 0 \\ 0 \\ 0 \\ 0 \end{bmatrix} \right\}$$

namely, the position state is in a 3-dimensional cone with aperture θ centered about the x axis, then the following constraint on closing/approaching

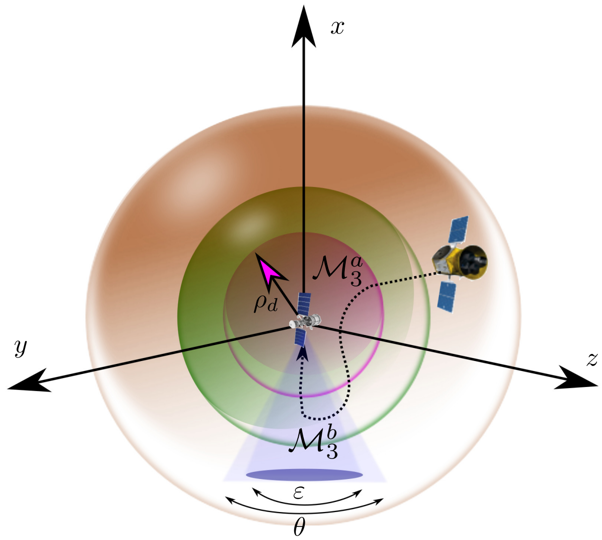

Figure 4: Constrains defining Phase III.

velocity [5] is satisfied:

$$\eta \in \mathcal{M}_3^c := \{ \eta \in \mathbb{R}^6 : \ \rho(\dot{x}, \dot{y}, \dot{z}) \leq V_{\max} \ \},$$

where $\rho(\dot{x}, \dot{y}, \dot{z}) := \sqrt{\dot{x}^2 + \dot{y}^2 + \dot{z}^2}$;

e) Phase IV constraints: When the chaser docks to the target (docked phase), the chaser-target dynamics are given as in (2) with $m_c + m_t$ in place of m_c under the constraint (4), where m_t is the mass of the target spacecraft located at the relocation position given by $(x, y, z) = (0, 0, 0)$. In addition, position measurements relative to a partner at location (x_p, y_p, z_p) are available, namely,

$$h(\eta) = \left[\arctan\left(\frac{r_x(x)}{r_y(y)}\right) \quad \arcsin\left(\frac{r_z(z)}{\rho(r_x, r_y, r_z)}\right) \quad \rho(r_x, r_y, r_z) \right], \tag{7}$$

where $r_x(x) = x - x_p, \ r_y(y) = y - y_p, \ r_z(z) = z - z_p, \ v \in \mathcal{N}^2(0, \sigma_4^2)$;

f) Time constraints: The following holds for the η-component $t \mapsto \eta(t)$ of each solution to the closed-loop system: for some $t_{2f} < t_{3f} < t_{4f}$ such that $t_{3f} \leq t_e$, $t_{4f} \leq t_f$, we have

(a) The chaser reaches the cone first, i.e.,

$$\eta(t_{2f}) \in \mathcal{M}_3^a \cap \mathcal{M}_3^b \ \text{ and } \ \rho(x(t_{2f}), y(t_{2f}), z(t_{2f})) = \rho_d;$$

[5]This is the "maximum closing velocity constraint."

(b) Next, the chaser docks on the target no later than t_{3f} time units, i.e.,

$$\eta(t_{3f}) \in \mathcal{M}_3^c = \left\{\eta \in \mathbb{R}^6 \;:\; \eta = 0\;\right\};$$

(c) Once docked, the docked chaser (or chaser-target) reaches the partner location no later than t_{4f} time units, i.e.,

$$\eta(t_{4f}) \in \mathcal{M}_4$$

where

$$\mathcal{M}_4 := \left\{\eta \in \mathbb{R}^6 : (x,y,z) = (x_p, y_p, z_p), (\dot{x}, \dot{y}, \dot{z}) = (0,0,0)\right\}.$$

$\triangle$

Remark 3.1. *The values of the constants m_c, m_t, μ, r_o, $u_{\max}$, and (x_p, y_p, z_p) are imposed by the vehicles and their environment. The constants $\rho_{\max}$, ρ_r, ρ_d, $\overline{V}$, $V_{\max}$, θ, t_f, and t_e are imposed by the mission and the desired performance.*

To define the dynamics of the systems to control under the above constraints in **Problem** 1, we define the following functions and sets (see Figure 3, Figure 4): with $\varepsilon \in (0, \theta)$, $\delta_{2b}^* > 0$,

$$\begin{aligned}
\mathcal{M} &:= \mathcal{M}_2 \cup \mathcal{M}_3^a = \left\{\eta \in \mathbb{R}^6 \;:\; \rho(x,y,z) \in [0, \rho_r)\right\}, \\
\mathcal{X}_{los} &:= \mathcal{M}_3^a \cap \mathcal{M}_3^b(\theta), \\
\mathcal{X}_{los}^{\varepsilon} &:= \mathcal{M}_3^a \cap \mathcal{M}_3^b(\theta - \varepsilon), \\
\mathcal{X}_{los}^{\varepsilon\delta} &:= \left((\mathcal{X}_{los}^{\varepsilon} + \delta_{2b}^*\mathbb{B}) \cap \mathcal{M}_3^b(\theta - \varepsilon)\right) \setminus \mathcal{X}_{los}^{\varepsilon}, \\
h_1(\eta) &:= \begin{bmatrix} \arctan\left(\frac{y}{x}\right) \\ \arcsin\left(\frac{z}{\rho(x,y,z)}\right) \\ \rho(x,y,z) \end{bmatrix} && \forall \eta \in \mathcal{M} \cup \mathcal{M}_1, \\
h_2(\eta) &:= h_1(\eta) && \forall \eta \in \mathcal{M}, \\
h_3(\eta) &:= h_1(\eta) && \forall \eta \in \mathcal{M}, \\
h_4(\eta) &:= \begin{bmatrix} \arctan\left(\frac{r_x(x)}{r_y(y)}\right) \\ \arcsin\left(\frac{r_z(z)}{\rho(r_x, r_y, r_z)}\right) \\ \rho(r_x, r_y, r_z) \end{bmatrix} && \forall \eta \in \mathcal{M},
\end{aligned}$$

Note, the dynamics of the chaser are given by the plant

$$\left.\begin{aligned}
\dot{\eta} &= A\eta + Bu \\
y_a &= h_P(\eta) := \begin{array}{ll} \begin{bmatrix} h_1(\eta) \\ h_0(\eta) \end{bmatrix} & \text{if } \eta \in \mathcal{M}_1 \\ \;\; h_1(\eta) & \text{if } \eta \in \mathcal{M} \end{array}
\end{aligned}\right\} (\eta, u) \in C_P \times \mathcal{U}_P \tag{8}$$

where $C_P := (((\mathcal{M} \cup \mathcal{M}_1) \setminus \mathcal{X}_{los}) \cup (\mathcal{X}_{los} \cap \mathcal{M}_3^c))$. The virtual output function h_0 is defined to capture the lack of range measurements when in $\mathcal{M}_1$: for some small $\gamma > 0$, $h_0(\eta)$ is zero for each $\eta \in \mathcal{M}_1 \setminus (\mathcal{M} + \gamma\mathbb{B})$, and equal to $\sqrt{x^2+y^2+z^2}$ for each $\eta \in \mathcal{M}$. In addition, h_1, h_2, h_3, and h_4, define the range and angle measurements as in (5). Similarly, the constrained dynamics of the chaser-target are

$$\left.\begin{array}{rcl} \dot{\eta} & = & A\eta + B_R u \\ y_b & = & h_R(\eta) := h_4(\eta) \end{array}\right\} \qquad (\eta, u) \in C_R \times \mathcal{U}_P \tag{9}$$

where $B_R := \frac{1}{m_c+m_t}(\mathbf{0}_{3\times 3}, I_3)$ $\quad C_R := \mathcal{M}$, and $\mathcal{U}_P$ is defined in (4).

4. General Hybrid Feedback Control Strategy

4.1. General strategy to solve **Problem** 1

Next, we propose an algorithm that supervises multiple hybrid controllers that are designed to cope with the individual constraints and to satisfy the desired temporal properties. The supervising algorithm is modeled as a hybrid system, which we denote by $\mathcal{H}_s$, and is in charge of supervising the following individual hybrid controllers:

- Hybrid controller for rendezvous from distances far from target (Phase I): this controller is denoted $\mathcal{H}_{c,1}$ and its goal is to steer the chaser to a point in the interior of $\mathcal{M}$, in particular, from points in the compact set $\mathcal{M}_1 \cap \mathcal{M}_0$;

- Hybrid controller for rendezvous in close-proximity to target (Phase II): this controller is denoted $\mathcal{H}_{c,2}$ and its goal is to steer the chaser to a point in the interior of $\mathcal{X}_{los}$, in particular, from points in $\mathcal{M}_2$;

- Hybrid controller for docking to target (Phase III): this controller is denoted $\mathcal{H}_{c,3}$ and its goal is to steer the chaser to nearby $\eta = 0$ from points in $\mathcal{M}_2 \cup \mathcal{M}_3^a$;

- Hybrid controller for relocation of target (Phase IV): this controller is denoted $\mathcal{H}_{c,4}$ and its goal is to steer the chaser-target from nearby $\mathcal{M}_3^c$ to a neighborhood of the partner position (x_p, y_p, z_p).

The operations described above are subject to the constraints stated in **Problem** 1. Each of the hybrid controllers operates in specific regions of the state space. These regions along with the goals of the individual hybrid controllers are formalized next. Note that the tasks performed by the controllers $\mathcal{H}_{c,3}$ and $\mathcal{H}_{c,4}$ are practical, in the sense that the trajectories η are steered from and to neighborhoods of the desired sets respectively. With this strategy, we have the following result.

Theorem 4.1. *Given the parameters listed in* **Problem 1** *and subject to the constraints therein, suppose there exist positive constants* δ_1, δ_1^*, δ_2, δ_{2a}^*, δ_{2b}^*, δ_3,

δ_3^*, δ_4, δ_4^*, *and* ε, *such that* $\delta_1 \in (0, \min\{\delta_1^*, \rho_r - \rho_d\})$, $\delta_2 \in (0, \delta_{2a}^*)$, $\delta_3^* \in (0, \rho_d)$, $\delta_3 \in (0, \delta_3^*)$, *closed sets* $\mathcal{A}_1$, $\mathcal{A}_2$, *and* $\mathcal{A}_4$ *satisfying*

$$\begin{array}{lcl} \mathcal{A}_1 + \delta_1^* \mathbb{B} & \subset & \mathcal{M}, \\ \mathcal{A}_2 + \delta_{2a}^* \mathbb{B} & \subset & \mathcal{X}_{los}^{\varepsilon\delta}, \\ \mathcal{A}_4 + \delta_4 \mathbb{B} & \subset & (x_p, y_p, z_p, 0, 0, 0) + \delta_4^* \mathbb{B}, \end{array} \tag{10}$$

$(x_p, y_p, z_p, 0, 0, 0) \in \mathcal{A}_4$ *and*

1. *A well-posed hybrid controller* $\mathcal{H}_{c,1}$ *rendering* $\mathcal{A}_1 + \delta_1 \mathbb{B}$ *finite-time attractive from* $\mathcal{M}_1 \cap \mathcal{M}_0$ *within* T_1 *seconds;*

2. *A well-posed hybrid controller* $\mathcal{H}_{c,2}$ *rendering* $\mathcal{A}_2 + \delta_2 \mathbb{B}$ *finite-time attractive from* $\left\{ \eta \in \mathbb{R}^6 \ : \ \rho(x, y, z) \in [0, \rho_r - \delta_1] \ \right\}$ *within* T_2 *seconds;*

3. *A well-posed hybrid controller* $\mathcal{H}_{c,3}$ *capable of*

   (a) *steering* η *from* $\mathcal{A}_2 + \delta_2 \mathbb{B}$ *to* $\mathcal{X}_{los}^{\varepsilon}$ *within* T_{3a} *seconds;*

   (b) *rendering* $\mathcal{X}_{los}^{\varepsilon} \cup \mathcal{X}_{los}^{\varepsilon\delta}$ *forward invariant;*

   (c) *steering* η *from* $\mathcal{X}_{los}^{\varepsilon}$ *to* $\mathcal{A}_3 + \delta_3 \mathbb{B}$ *within* T_{3b} *seconds, where,* $\mathcal{A}_3 := \{(0, 0, 0, 0, 0, 0)\}$.

4. *A well-posed hybrid controller* $\mathcal{H}_{c,4}$ *rendering* $\mathcal{A}_4 + \delta_4 \mathbb{B}$ *finite-time attractive from* $\mathcal{A}_3 + \delta_3 \mathbb{B}$ *within* T_4 *seconds and* $\mathcal{A}_4$ *asymptotically stable, with the basin of attraction containing* $\mathcal{A}_4 + \delta_4 \mathbb{B}$.

5. $T_1 + T_2 + T_3 \leq t_e$ *and* $T_4 \leq t_f - t_e$.

Then, there exists a supervisor $\mathcal{H}_s$ *that solves*[6] **Problem 1** *and renders the set* $\mathcal{A}_4$ *asymptotically stable with basin of attraction containing* $\mathcal{M}_0$ *when projected to the* η *component of the state space. Furthermore, the set* $\mathcal{A}_4$ *is semiglobally practically robustly asymptotically stable for the closed-loop system with quantifiable margin of robustness* [7].

Note that Theorem 4.1 requires finite-time attractivity of neighborhoods of the sets $\mathcal{A}_1$, $\mathcal{A}_2$, $\mathcal{A}_3$, and $\mathcal{A}_4$, rather than finite-time attractivity of these sets themselves. The required finite-time attractivity property can be guaranteed using tools asymptotic stabilization of sets applied to the respective sets $\mathcal{A}_1$, $\mathcal{A}_2$, $\mathcal{A}_3$, and $\mathcal{A}_4$.

[6] Modulo the fact that the η converges to a δ_4^* neighborhood of the partner position.

[7] In Theorem 4.1, 'practical' means that the solutions to the closed-loop hybrid system in the presence of some small disturbances, converge $\delta_4 > 0$ close to the desired set $\mathcal{A}_4$ in a semiglobal manner, namely, when the solutions start from arbitrary compact sets of initial conditions. Also, the value of δ_4 can be made arbitrarily small but not necessarily zero.

5. Individual controller design

Before formalizing the individual controller design, since the chaser is relatively far away from the target, and only range and angle measurements are available, first an observer-based LQR controller using hybrid Kalman filter is implemented in Phase I with the additional feedforward term $\Gamma(\eta)$. Precisely, following [37], [38, Chapter 14], we feedforward the term

$$\Gamma(\eta) := \left(\mathbf{0}_{1\times 3}, -2n^2 x + \frac{\mu}{r_o^2} - \frac{\mu}{r_d^3}(r_o + x), n^2 y - \frac{\mu}{r_d^3} y, n^2 z - \frac{\mu}{r_d^3} z \right).$$

The controllers in the Phases II-IV sections are designed considering that the state $\eta \in \mathbb{R}^6$ is available for feedback. Note that the state $\eta \in \mathbb{R}^6$ in Phases II-IV can be estimated with observer (hybrid Kalman) without the feedforward term due to the closer relative distance between the chaser and the target spacecraft.

To establish the properties in Theorem 4.1, we explicitly construct a supervisor $\mathcal{H}_s$ guaranteeing the stated properties. We start by characterizing the properties of the individual hybrid controllers, followed by the individual controller design.

5.1. Hybrid controller for Phase I

The hybrid controller $\mathcal{H}_{c,1}$ renders an inflation of the closed set $\mathcal{A}_1$ finite-time attractive for the solution components η starting from $\mathcal{M}_1 \cap \mathcal{M}_0$. The inflation is given by the set $\mathcal{A}_1 + \delta_1 \mathbb{B}$ with $\delta_1 \in (0, \delta_1^*)$, where $\delta_1^* > 0$ satisfies (10). Namely, the basin of attraction induced by $\mathcal{H}_{c,1}$ in η-space is $\mathcal{B}_1^\eta$ and contains $\mathcal{M}_1 \cap \mathcal{M}_0$. When this property holds, the components η of solutions with $\mathcal{H}_{c,1}$ will reach $\mathcal{M}$ in finite time due to $\mathcal{A}_1$ being in the interior of $\mathcal{M}$. The neighborhood of size δ_1^* in (10) enables the supervisor to use measurements given by h_2 to detect when η is inside $\mathcal{M}$. For this purpose, we define the set of η points that trigger switches in the supervisor from using $\mathcal{H}_{c,1}$ to using $\mathcal{H}_{c,2}$ as

$$D_{12} := \left\{ \eta \in \mathbb{R}^6 \ : \ \rho(x, y, z) \in [0, \rho_r - \overline{\delta}_1 \ \right\}],$$

where, $\overline{\delta}_1 \in (0, \min\{\delta_1^*, \rho_r - \rho_d\})$ is such that

$$\mathcal{A}_1 + \delta_1 \mathbb{B} \subset D_{12} \text{ and } \mathcal{M} \setminus D_{12} \subset \mathcal{M}_2.$$

The latter condition guarantees that switches from using $\mathcal{H}_{c,1}$ to using $\mathcal{H}_{c,2}$ occur inside $\mathcal{M}_2$.

Due to the presence of noise or wrong initializations, switches back to $\mathcal{H}_{c,1}$ may need to be triggered. Using measurements given by h_2, such switches will occur nearby the boundary of $\mathcal{M}$ and away from D_{12}. We refer to this set as the recovery set of the supervisor and define it as

$$D_{r1} := \left\{ \eta \in \mathbb{R}^4 \ : \ \rho(x, y, z) \in [\rho_r - \delta_{r1}, \rho_r] \ \right\},$$

where, $\delta_{r1} \in (0, \overline{\delta}_1)$. Figure 5 sketches these constructions.

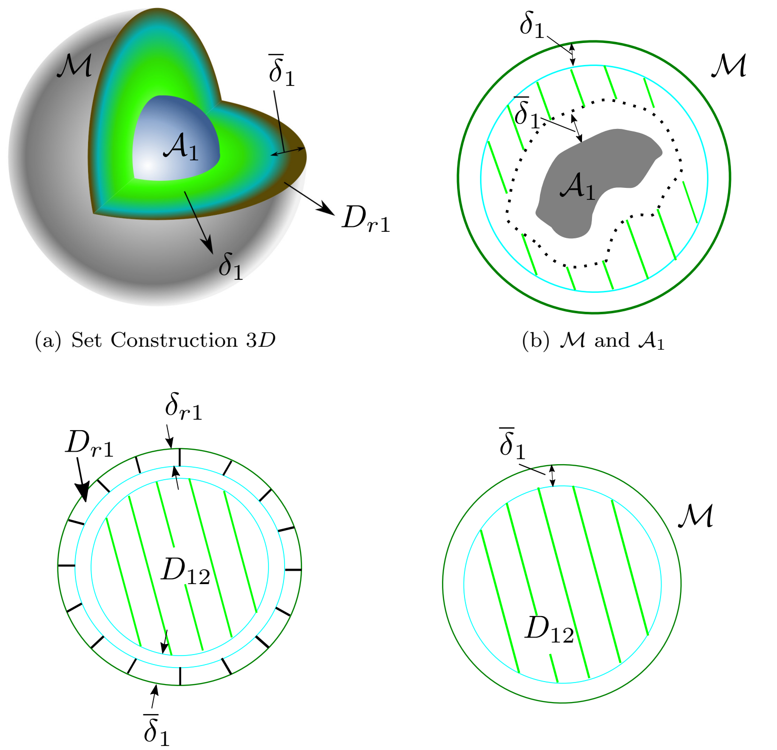

(a) Set Construction $3D$ (b) $\mathcal{M}$ and $\mathcal{A}_1$

(c) $\mathcal{M}$ and D_{r1} (d) $\mathcal{M}$ and D_{12}

Figure 5: 2D representation of the set constructions for $\mathcal{H}_{c,1}$.

5.1.1. An observer-based LQR design of $\mathcal{H}_{c,1}$

The controller $\mathcal{H}_{c,1}$ is designed such that the inflated closed set $\mathcal{A}_1+\delta_1\mathbb{B} \subset \mathcal{M}$ is finite-time attractive for the initial conditions starting from basin of attraction induced by $\mathcal{H}_{c,1}$ in η space, as outlined in Section 5.1. Since the chaser is relatively far away from the target in Phase I, we implement a hybrid Kalman as discussed in the beginning of Section 5. This hybrid observer (that resembles a continuous-discrete extended Kalman filter) with state $\chi_e := (\eta_e, S, \tau) \in \mathbb{R}^n \times \Pi_{\geq 0} \times [0, T_{\max}] =: X_e$, $U \subset \mathcal{U}_P$, is given as follows:

$$\begin{array}{rclcrcl} \dot{\chi}_e & = & f_e(\chi_e, u) & \qquad & (\chi_e, u) & \in & C_e \times U, \\ \chi_e^+ & = & g_e(\chi_e) & & \chi_e & \in & D_e, \end{array} \tag{11}$$

where the maps $f_e : X_e \times U \to X_e$, $g_e : X_e \to X_c$ and the sets $C_e \subset X_e$, $D_e \subset X_e$ are

$$f_e(\chi_e, u) := \begin{bmatrix} A\eta_c + Bu + \Gamma(\eta_e) \\ -\widetilde{A}^\top S - S\widetilde{A} - SQS \\ 1 \end{bmatrix} \forall\ (\chi_e, u) \in C_e \times U,$$

$$g_e(\chi_e) := \begin{bmatrix} \eta_e + (\star_3)^{-1} H^\top (\frac{R}{\tau})^{-1}(y - h(\eta_e)) \\ \star_3 \\ 0 \end{bmatrix} \forall\ \chi_e \in D_e,$$

$C_e := \mathbb{R}^n \times \Pi_{\geq 0} \times [0, T_{\max}]$, $D_e := \mathbb{R}^n \times \Pi_{\geq 0} \times [T_{\min}, T_{\max}]$; $\widetilde{A} := \frac{\partial f(\eta_e, u)}{\partial \eta_e}$, $f(\eta_e, u) := A\eta_e + Bu + \Gamma(\eta_e)$, $H := \frac{\partial h}{\partial \eta}\big|_{\eta_e}$, $\star_3 := S + H^\top (\frac{R}{\tau})^{-1} H$, where $\frac{\partial f(\eta_e, u)}{\partial \eta_e}$ is the Jacobian of f with respect to η_e evaluated at (η_e, u); the $Q \in \Pi_{>0}$ and $R \in \Pi_{>0}$ are similar to the covariance matrices of the state noise and output noise in the stochastic context, respectively. The components of the observer state χ_e consists of, the estimated system state η_e, the error information matrix S, and a timer τ that triggers measurement errors obtained at isolated time instances t_k, $k \in \mathbb{N}$. Next, we design a feedback controller, to which the state estimates η_e is fed given as follows:

$$u = -K^e \eta_e - m_c^2 B^\top \Gamma(\eta_e). \tag{12}$$

Since the order of $\Gamma(\eta)$ is small relative to the state η, the controller gain matrix $K^e \in \mathbb{R}^{6\times 6}$ is designed by the LQR method(infite horizon), initially ignoring the nonlinear component $\Gamma(\eta)$ such that $(A - BK^e)$ is Hurwitz. Next, feedback linearization is implemented to compensate for the omitted nonlinearities.

Therefore, given the dynamics of the chaser in (8), with the observer (11) and the controller feedback (12), the resulting hybrid closed-loop system $\mathcal{H}_1 := (C_1, f_1, D_1, g_1)$ has state $\chi := (\eta, \eta_e, S, \tau) \in \mathbb{R}^n \times X_e =: X$ and dynamics given by

$$\begin{array}{rclcrcl} \dot{\chi} & = & f_1(\chi, u) & & (\chi, u) & \in & C_1 \times U, \\ \chi^+ & = & g_1(\chi) & & \chi & \in & D_1, \end{array} \tag{13}$$

where $f_1 : X \times U \to X$, $g_1 : X \to X$ and the sets $C_1 \subset X$, $D_1 \subset X$ are

$$f_1(\chi, u) := \begin{bmatrix} A\eta + Bu + \Gamma(\eta) \\ A\eta_e + Bu + \Gamma(\eta_e) \\ -\widetilde{A}^\top S - S\widetilde{A} - SQS \\ 1 \end{bmatrix} \forall\ (\chi, u) \in C_1 \times U,$$

$$g_1(\chi) := \begin{bmatrix} \eta \\ \eta_e + (\star_3)^{-1} H^\top (\frac{R}{\tau})^{-1}(y - h(\eta_e)) \\ \star_3 \\ 0 \end{bmatrix} \forall\ \chi \in D_1,$$

$C_1 := \mathbb{R}^n \times C_e$, $D_1 := \mathbb{R}^n \times D_e$. Stability analysis for this hybrid closed-loop system $\mathcal{H}_1$ with sufficient conditions involving the parameters defining the window for measurements is presented in [39]. In this reference, convergence of the error dynamics to zero is achieved via Lyapunov analysis for hybrid systems.

5.2. Hybrid controller for Phase II

The hybrid controller $\mathcal{H}_{c,2}$ renders an inflation of the closed set $\mathcal{A}_2$ finite-time attractive for the solution components η starting from D_{12}. The inflation is given by the set $\mathcal{A}_2 + \delta_2\mathbb{B}$ with $\delta_2 \in (0, \delta_{2a}^*)$, where $\delta_{2a}^* > 0$ satisfies

$$\mathcal{A}_2 + \delta_{2a}^*\mathbb{B} \subset \mathcal{X}_{los}^{\varepsilon\delta} \tag{14}$$

for some $\delta_{b2}^* > 0$. Namely, the basin of attraction induced by $\mathcal{H}_{c,2}$ in η space is $\mathcal{B}_2^\eta$ and contains D_{12}. When this property holds, the components η of such solutions will reach in finite time a nearby point outside $\mathcal{X}_{los}$ that is within the cone, namely, a point in $\mathcal{X}_{los}^{\varepsilon\delta}$. By steering η to a point outside of $\mathcal{X}_{los}$, the hybrid controller $\mathcal{H}_{c,2}$ does not need to satisfy the maximum closing velocity constraint imposed within $\mathcal{X}_{los}$ (this task is relayed to $\mathcal{H}_{c,3}$). Unlike the construction of $\mathcal{H}_{c,1}$, the supervisor will trigger switches that stop using $\mathcal{H}_{c,2}$ and start using $\mathcal{H}_{c,3}$ when η in $\mathcal{A}_2 + \delta_2\mathbb{B}$. Then, we define $D_{23} := \overline{\mathcal{A}_2 + \delta_2\mathbb{B}}$. Switches back to $\mathcal{H}_{c,2}$ may need to be triggered due to the presence of perturbations or wrong initializations. Let

$$\mathcal{X}_{los}^\delta := \big((\mathcal{X}_{los} + \delta_{2b}^*\mathbb{B}) \cap \mathcal{M}_3^b(\theta)\big) \setminus \mathcal{X}_{los}.$$

Using measurements given by h_3, such switches will occur right outside of $\mathcal{X}_{los} \cup \mathcal{X}_{los}^\delta$. Then, the recovery set of the supervisor for this controller is given by $D_{r2} := \overline{\mathcal{M} \setminus (\mathcal{X}_{los} \cup \mathcal{X}_{los}^\delta)}$. Figure 6 sketches these constructions.

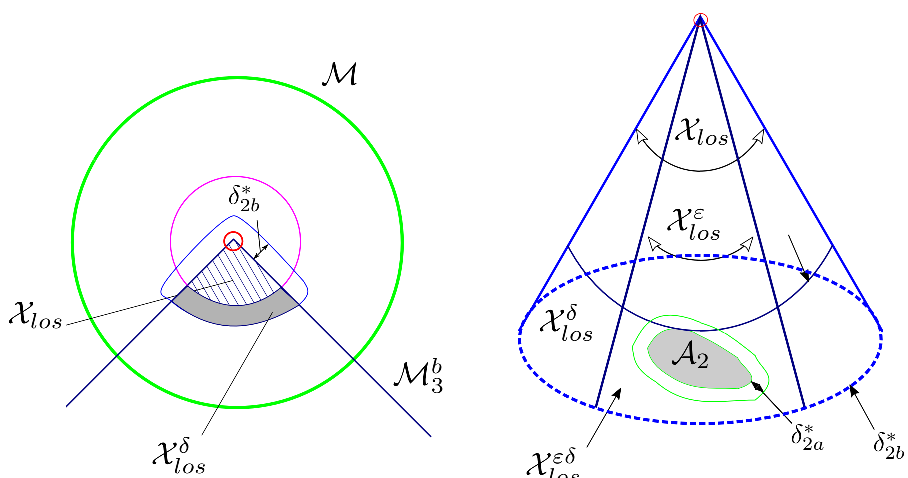

(a) $\mathcal{X}_{los}^\delta$ (b) $\mathcal{X}_{los}^{\varepsilon\delta}$

Figure 6: Set constructions for $\mathcal{H}_{c,2}$ and $\mathcal{H}_{c,3}$.

5.2.1. A logic-based line-of-sight controller of $\mathcal{H}_{c,2}$

Let us consider the chaser dynamics in (8). In this phase, we consider that the state $\eta \in \mathbb{R}^6$ is available for feedback as outlined in the beginning of Section 5. The hybrid controller $\mathcal{H}_{c,2}$ is designed to render the inflated closed set $\mathcal{A}_2 + \delta_2\mathbb{B}$ finite-time attractive for the solution components η starting from D_{12}. Since the $x-y$ plane dynamics for the chaser are decoupled from z plane, we design individual controllers for the motion on each of these planes.

a) <u>*Controller for $x-y$ plane motion:*</u> Let us consider that the out-of-plane states $(z, \dot{z}) = (0, 0)$. Thus, the chaser dynamics in (8) and the associated parameters defined in Section 2 are reduced to 2D $x-y$ plane motion. The output of this system from (8) is given by $y = h_1(\eta) = (\alpha, \rho)$, where, $\alpha = \arctan\left(\frac{y}{x}\right)$, $\rho = \sqrt{(x^2+y^2)}$. Using the fact that initial conditions of the chaser belong to D_{12}, we exploit the ideas in [14] (in particular, the change of coordinates [14, equation 1-18]). In this design, a proportional-derivative control law that guides the chaser to dock with the target at a desired docking direction (α^*) and position (ρ^*) is proposed. Next, we introduce a logic variable to handle the topological obstruction of stabilizing a set on a manifold. In fact, with a continuous state feedback law, there will be antipodal points to $\mathcal{A}_2$ (nearby $\alpha = 0$) from where the chaser can move either left or right to reach the desired line of sight. While, alternatively, a discontinuous controller can be designed, such a discontinuous controller would not be robust to small measurement noise as previously shown in literature [40]. We design a logic-based hybrid controller that steers the chaser either clockwise or counter-clockwise to take shortest route and reach a point in $\mathcal{X}_{los}^{\varepsilon\delta}$ and be robust to small perturbations. To this end, let us consider a hybrid feedback similar to the hybrid controller in [40], that depends on the logic variable $\ell \in \{-1, 1\}$, along with a feed-forward term that depends on the reference input $(\alpha^*, \rho^*) \in \mathbb{R}^2$. The proposed hybrid controller $\mathcal{H}_{c,2}$ is given as following.

$$\begin{aligned} \dot{\ell} &= 0 && (\eta, \ell) \in C_2, \\ \ell^+ &= -\ell && (\eta, \ell) \in D_2, \\ u &= \kappa_2(\eta), \end{aligned} \tag{15}$$

where $\kappa_2(\eta) := \begin{bmatrix} \cos(\alpha) & -\sin(\alpha) \\ \sin(\alpha) & \cos(\alpha) \end{bmatrix} \begin{bmatrix} a_\rho \\ a_\alpha \end{bmatrix}$, $a_\rho = u_\rho + n_\rho$, and

$a_\alpha = u_\alpha + n_\alpha$. Specifically, with the terms $\rho_e := \rho - \rho^*$, $\alpha_e := \alpha - \ell\alpha^*$, $\dot{\rho}_e = \dot{\rho} = v_\rho$, $\dot{\alpha} = \frac{1}{\rho}(-\dot{x}\sin(\alpha) + \dot{y}\cos(\alpha))$, the terms u_ρ, u_α, n_ρ, n_α are defined as follows.

$$\begin{aligned} u_\rho &= -k_1\dot{\rho}_e - k_2\rho_e, \quad u_\alpha = -\rho(k_3\dot{\alpha}_e + k_4\alpha_e), \\ n_\rho &= -[3n^2x + \dot{y}(2n+\dot{\alpha})]\cos(\alpha) + \dot{x}(2n+\dot{\alpha})\sin(\alpha), \\ n_\alpha &= [3n^2x + \dot{y}(2n+\dot{\alpha})]\sin(\alpha) + \dot{x}(2n+\dot{\alpha})\cos(\alpha) + v_\rho\dot{\alpha}, \end{aligned}$$

where k_1, k_2, k_3, k_4 are positive constants, $v_\rho = \dot{x}\cos(\alpha) + \dot{y}\sin(\alpha)$. This construction is obtained by changing to a coordinate system (in polar coordinates) that is fixed to the target spacecraft with its origin moving at a constant angular rate n; see [14]. The sets with the controller parameter $\varrho \in (0, \pi)$ are given as follows.

$$\begin{array}{rcl} C_2 & := & \{(\eta, \ell) \in \mathbb{R}^4 \times \{-1, 1\} : \ell\alpha \geq -\varrho\}, \\ D_2 & := & \{(\eta, \ell) \in \mathbb{R}^4 \times \{-1, 1\} : \ell\alpha \leq -\varrho\}. \end{array} \tag{16}$$

With the proposed hybrid controller (15), and the chaser dynamics (8) without the out-of-plane dynamics, i.e., $(z, \dot{z}) = (0, 0)$, the resulting closed-loop hybrid system denoted $\mathcal{H}_2 := (C_2, f_2, D_2, g_2)$ has state $\xi = (\eta, \ell) \in \mathbb{R}^4 \times \{-1, 1\} =: \mathcal{X}$ and hybrid dynamics

$$\begin{array}{rclcl} \dot{\xi} & = & f_2(\xi) & \xi & \in C_2, \\ \xi^+ & = & g_2(\xi) & \xi & \in D_2. \end{array} \tag{17}$$

The flow and jump sets satisfy $C_2 \cup D_2 = \mathcal{X}$ and the maps $f_2 : \mathcal{X} \to \mathcal{X}$ and $g_2 : \mathcal{X} \to \mathcal{X}$ are given by

$$\begin{array}{l} f_2(\eta, \ell) := \begin{bmatrix} A\eta + B\kappa_2(\ell\eta) \\ 0 \end{bmatrix} \quad \forall (\eta, \ell) \in C_2, \\ g_2(\eta, \ell) := \begin{bmatrix} \eta \\ -\ell \end{bmatrix} \quad \forall (\eta, \ell) \in D_2. \end{array} \tag{18}$$

The resulting hybrid feedback is such that, from points in C_2 nearby $\alpha = 0$, with $\varrho \in (0, \pi)$, it steers the chaser clockwise to $-\alpha^*$ if $\alpha < \varrho$ and counter-clockwise to α^* if $\alpha > -\varrho$. Due to the design of the hybrid feedback (15) - (16), this hybrid system has the compact set

$$\mathcal{A}_2 := \{\xi \in \mathcal{X} : \rho = \rho^*, \alpha = \ell\alpha^*\}, \tag{19}$$

globally asymptotically stable. Next, the hybrid closed-loop system $\mathcal{H}_2$ satisfies the hybrid basic conditions (see [35, Proposition 6.10]) and our result for this controller is as follows.

Theorem 5.1. *The set $\mathcal{A}_2$ in* (19) *is globally asymptotically stable for the closed-loop system $\mathcal{H}_2$.*

For the hybrid closed-loop system (17), we first show that every complete solution to it converges to $\mathcal{A}_2$. For this purpose, we use the invariance principle for hybrid systems in [35] for which $\mathcal{H}_2$ has to satisfy the hybrid basic conditions, which is already the case due to its construction. After that, since $\mathcal{H}_2$ satisfies the hybrid basic conditions, following [35, Proposition 6.10], we can conclude that every maximal solution to the hybrid system is complete, in this way showing asymptotic stability of $\mathcal{A}_2$ for $\mathcal{H}_2$.

See Appendix A for the details on the proof.

b) Controller for z plane motion: Let us consider the z-plane dynamics from the 3D chaser dynamics in (8). These out-of-plane dynamics with state $\eta_z = (z, \dot{z}) \in \mathbb{R}^2$ and input $u_z \in \mathbb{R}$ are given as following;

$$\dot{\eta}_z = A_z \eta_z + B_z u_z, \tag{20}$$

where, $A_z = \begin{bmatrix} 0 & 1 \\ -n^2 & 0 \end{bmatrix}$, $B_z = (0, \frac{1}{m_c})$. The main result for this controller is to asymptotically stabilize the set $\mathcal{A}_{3,z} := \{(z, \dot{z}) \in \mathbb{R}^2 : z = 0, \dot{z} = 0, \}$. A control law for such a maneuver is given by a linear continuous-time state feedback as follows:

$$\kappa_{2,z}(z, \dot{z}) := -K_{2,z}(z, \dot{z}), \tag{21}$$

where, the controller gain $K_{2,z}$ in (21) is designed using the LQR (infinite horizon) method such that $(A_z - B_z K_{2,z})$ is Hurwitz.

Remark 5.2. *In the simulations results presented in Section 7, the controller gain $K_{2,z}$ is designed by trial and error to satisfy the maximum thrust constraint and in addition$\sqrt{x^2 + y^2} > \rho_{xy}$, $\rho_{xy} > \rho_d$. This additional constraint restricts the out of plane motion to remain out of $\mathcal{M}_3^a$ region. Notice that this constraint avoids the scenario of chaser crashing into the target spacecraft. Alternately, control techniques that include such constrains implicitly in the modeling can also be considered.*

5.3. Hybrid controller for Phase III

The hybrid controller $\mathcal{H}_{c,3}$ steers η components of the solutions from $\mathcal{A}_2 + \delta_2\mathbb{B}$ to $\mathcal{X}_{los}^{\varepsilon}$ in finite time, render $\mathcal{X}_{los}^{\varepsilon} \cup \mathcal{X}_{los}^{\varepsilon\delta}$ forward invariant, and an inflation of the set $\mathcal{A}_3$ finite-time attractive. The inflation is given by the set $\mathcal{A}_3 + \delta_3\mathbb{B}$. This controller enforces the maximum closing velocity constraint within $\mathcal{X}_{los}$ as well. The finite separation between $\mathcal{A}_2 + \delta_2\mathbb{B}$ and $\mathcal{X}_{los}$ makes this task feasible as this controller will have time to slow down the chaser before reaching $\mathcal{X}_{los}^{\varepsilon}$ if needed. Then, switches of the supervisor to $\mathcal{H}_{c,4}$ are triggered when η is in $D_{34} := (\mathcal{A}_3 + \delta_3\mathbb{B}) \cap \mathcal{X}_{los}^{\varepsilon}$ which collects points that are δ_3-close to $\mathcal{A}_3$ with $\delta_3 \in (0, \delta_3^*)$, where δ_3^* is such that $(\mathcal{A}_3 + \delta_3^*\mathbb{B}) \cap \mathcal{X}_{los} \cap \mathcal{X}_{los}^{\delta} = \emptyset$ which is guaranteed by picking δ_3^* small enough. Figure 6 and Figure 7 sketch these constructions.

Uniting local and global design of $\mathcal{H}_{c,3}$: Let us consider the chaser dynamics in (8). In this phase, we once again consider that the state $\eta \in \mathbb{R}^6$ is available for feedback as outlined in the beginning of Section 5. The objective of the hybrid controller $\mathcal{H}_{c,3}$ is to steer the η components of the solutions from $\mathcal{A}_2 + \delta_2\mathbb{B}$ to $\mathcal{X}_{los}^{\varepsilon}$ in finite time. This controller is designed to induce forward invariance and to satisfy the closing speed constraints for the chaser. Hence, we do this in two stages, implementing logic-based algorithm that 'unites' two individual controllers.

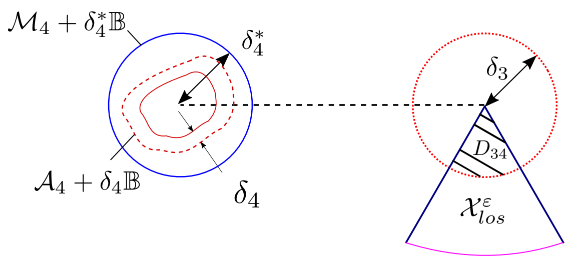

Figure 7: Set constructions for $\mathcal{H}_{c,3}$ and $\mathcal{H}_{c,4}$.

First, a controller with output κ_3^1, thrusts the chaser towards the reference way-point $\eta_r := (x_r, \mathbf{0}_{1\times 5})^\top \in \mathcal{X}_{los}^{\varepsilon}$ within T_{3a} seconds while guaranteeing forward invariance of $\mathcal{X}_{los}^{\varepsilon} \cup \mathcal{X}_{los}^{\varepsilon\delta}$. Second, a controller with output κ_3^2 implements a damping control law that guides the chaser from $\mathcal{X}_{los}^{\epsilon}$ to the inflated set $\mathcal{A}_3 + \delta_3 \mathbb{B}$ within T_{3b}, along the vertical axis and slowing down the vehicle so as to satisfy the closing speed constraint. To implement such a switch between two controllers, a dynamic feedback that depends on the logic variable $p \in \{1, 2\}$, along with a feedforward term that depends on the reference input $\eta_r^p \in \mathbb{R}^3$ is proposed. Such a hybrid controller is given as follows:

$$\begin{array}{lcll} \dot{p} & = & 0 & (\eta, p) \in C_3 \\ p^+ & = & 3 - p & (\eta, p) \in D_3 \\ u & = & \kappa_3^p(\eta, \eta_r^p) & \end{array} \tag{22}$$

where for each $p \in \{1, 2\}$, $\eta_r^2 = 0$,

$$\begin{aligned} \kappa_3^1(\eta, \eta_r^1) &= -K_3^1(\eta - \eta_r^1), \\ \kappa_3^2(\eta, \eta_r^2) &= \begin{bmatrix} 3n^2 - k_1 & 0 & -k_2 & 0 \\ 0 & -k_3 & 0 & -k_4 \end{bmatrix} \eta \end{aligned} \tag{23}$$

The sets, $C_3 = \cup_{p\in\{1,2\}} C_3^p \times \{p\}$, $D_3 = \cup_{p\in\{1,2\}} D_3^p \times \{p\}$, where the set C_3^1 is taken to be a compact neighborhood of the reference way-point η_r^1 that is contained in the basin of attraction of κ_3^2. The set D_3^2 is taken as a compact neighborhood of η_r^1 such that solutions using κ_3^1 that start in D_3^2 do not reach the boundary of C_3^1. Then, we define $C_3^2 = \overline{\mathbb{R}^4 \setminus D_3^2}$ and $D_3^1 = \overline{\mathbb{R}^4 \setminus C_3^1}$.

The data of the resulting hybrid closed-loop system, which includes the plant dynamics in (8), and the hybrid controller (22) is denoted by $\mathcal{H}_3 := (C_3, f_3, D_3, g_3)$. The dynamics of this hybrid closed-loop system are given as follows:

$$\begin{array}{lcll} (\dot{\eta}, \dot{p}) & = & f_3(\eta, p), & (\eta, p) \in C_3, \\ (\eta^+, p^+) & = & g_3(\eta, p), & (\eta, p) \in D_3. \end{array} \tag{24}$$

The flow and jump sets satisfy $C_3 \cup D_3 = \mathbb{R}^6 \times \{1, 2\}$ and the maps $f_3 : \mathbb{R}^6 \times \{1, 2\} \to \mathbb{R}^6 \times \{1, 2\}$ and $g : \mathbb{R}^6 \times \{1, 2\} \to \mathbb{R}^6 \times \{1, 2\}$ are given by

$$\begin{aligned} f_3(\eta, p) &:= \begin{bmatrix} A\eta + B\kappa_3^p(\eta, \eta_r^p) \\ 0 \end{bmatrix} \quad && \forall (\eta, p) \in C_3, \\ g_3(\eta, p) &:= \begin{bmatrix} \eta \\ 3 - p \end{bmatrix} && \forall (\eta, p) \in D_3. \end{aligned} \tag{25}$$

With the construction above, the hybrid closed-loop system $\mathcal{H}_3$ renders the set $\mathcal{A}_3$ uniformly globally asymptotically stable. (see [35, Example 3.23]).

Remark 5.3. *Particular constructions used in the forthcoming simulations are as given in* (23)*, where* $K_3^1 \in \mathbb{R}^{6\times 6}$ *is designed via LQR(infinite horizon) and* k_1*,* k_2*,* k_3*, and* k_4 *are positive constants such that* $(A - BK_3^p)$*,* $p \in \{1, 2\}$ *is Hurwitz.*

5.4. Hybrid controller for Phase IV

The hybrid controller $\mathcal{H}_{c,4}$ performs a maneuver in finite time from points in D_{34} to nearby $\mathcal{M}_4$ which is an isolated point. Due to the presence of noise, steering the state to an isolated point is not practical, and hence we design $\mathcal{H}_{c,4}$ to steer η in finite time to a point in $\mathcal{M}_4 + \delta_4^*\mathbb{B}$, where $\delta_4^* > 0$.

For this purpose, we propose a controller that renders the set $\mathcal{A}_4$ asymptotically stable and the set $\mathcal{A} + \delta_4\mathbb{B}$ finite-time stable, where $\delta_4 > 0$ is such that

$$\mathcal{A}_4 + \delta_4\mathbb{B} \subset \mathcal{M}_4 + \delta_4^*\mathbb{B}, \qquad \mathcal{M}_4 \subset \mathcal{A}_4$$

In particular, this construction assures some robustness to small perturbations. Figure 7 sketches these constructions.

5.4.1. An LQR design of $\mathcal{H}_{c,4}$

In Phase IV, the controller $\mathcal{H}_{c,4}$ has to steer the docked chaser-target from points in D_{34} to $\mathcal{M}_4 + \delta_4\mathbb{B}$, $\delta_4 > 0$, in finite time. To this end, let us consider the relative motion dynamics in (9). A control law for such a maneuver is given by a linear continuous-time state feedback as $\kappa_4(\eta) := -K_4(\eta - \eta_{r,4})$, where $\eta_{r,4} := (x_p, y_p, z_p, 0, 0, 0)$. Hence, the resulting closed-loop hybrid system, denoted $\mathcal{H}_4 := (C_4, f_4, D_4, g_4)$, has data given by

$$\dot{\eta} = f_4(\eta) \quad = \quad A\eta + B_R\kappa_4(\eta) \qquad \forall \eta \in C_4, \tag{26}$$

where $C_4 := \mathbb{R}^4$, $D_4 := \emptyset$ and arbitrary g_4 (that is, no jumps). The main result for this controller is to asymptotically stabilize the set $\mathcal{A}_4$ in (10). Hence, the controller gain $K_4 \in \mathbb{R}^{6\times 6}$ in (26) is designed using the LQR (infinite horizon) method so that $(A - B_R K_4)$ is Hurwitz. By trial and error, the gain K_4 is designed to satisfy the maximum thrust constraint.

6. Hybrid Supervisor

The supervisor (see Figure 8) employs the constructions Sections 5.1-5.4 to implement the following logic:

- Apply $\mathcal{H}_{c,1}$ when η is in $\overline{(\mathcal{M}_1 \cup \mathcal{M}) \setminus D_{12}}$;
- While applying $\mathcal{H}_{c,1}$, switch to $\mathcal{H}_{c,2}$ if η is in D_{12};
- Apply $\mathcal{H}_{c,2}$ in $\overline{\mathcal{M} \setminus D_{r1}}$;
- While applying $\mathcal{H}_{c,2}$, switch to $\mathcal{H}_{c,1}$ if η is in D_{r1};

- While applying $\mathcal{H}_{c,2}$, switch to $\mathcal{H}_{c,3}$ if η is in D_{23};
- Apply $\mathcal{H}_{c,3}$ if η is in $\mathcal{X}_{los}^{\varepsilon} \cup \mathcal{X}_{los}^{\varepsilon\delta}$;
- While applying $\mathcal{H}_{c,3}$, switch to $\mathcal{H}_{c,2}$ if η is in D_{r2};
- While applying $\mathcal{H}_{c,3}$, switch to $\mathcal{H}_{c,4}$ if η is in D_{34};
- Apply $\mathcal{H}_{c,4}$ and let η converge to $\mathcal{A}_4 + \delta_4\mathbb{B}$.

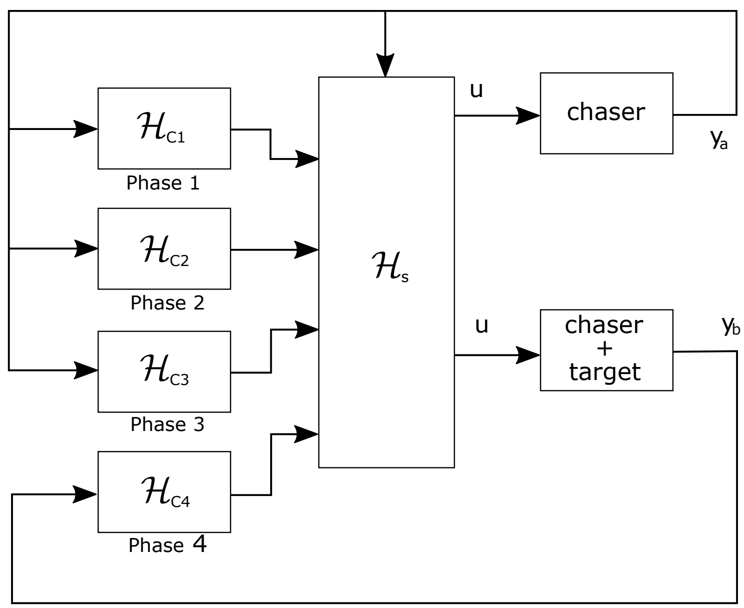

Figure 8: Hybrid feedback control solution.

A hybrid system implementing this logic is defined next. Let $q \in Q := \{1, 2, 3, 4\}$ be a logic state denoting the controller currently being applied. Then, for the nominal case, the hybrid supervisor has the following dynamics

$$\begin{aligned} \dot{q} &= 0 & \qquad (q, u_s) &\in C_s \\ q^+ &= G_s(q, u_s) & \qquad (q, u_s) &\in D_s \end{aligned}$$

with output $y_s = \kappa_c(q, u_s)$, where

- $\kappa_c(q, \cdot)$ is the output of $\mathcal{H}_{c,q}$;
- $u_s = y_a$ when $q \neq 4$, and $u_s = y_b$ when $q = 4$ – note that when $\eta \in \mathcal{M}$ and $q \neq 4$, $u_s = \eta$ in the nominal case;

- $C_s := \bigcup_{q\in Q} (\{q\} \times C_q)$ and $D_s = \bigcup_{q\in Q} (\{q\} \times D_q)$ where

$$\begin{aligned} C_1 &:= \overline{(\mathcal{M}_1 \cup \mathcal{M}) \setminus D_{12}}, \;\; C_2 \;:=\; \overline{\mathcal{M} \setminus D_{r1}} \\ C_3 &:= \mathcal{X}^{\varepsilon}_{los} \cup \mathcal{X}^{\varepsilon\delta}_{los}, \;\; C_4 \;:=\; \mathcal{M} \cup \mathcal{M}_1 \\ D_1 &:= D_{12}, \; D_2 \;:=\; D_{r1} \cup D_{23} \\ D_3 &:= D_{r2} \cup D_{34}, \; D_4 \;:=\; \emptyset \end{aligned}$$

- the jump map G_s is defined as

$$G_s(q, u_s) = \begin{cases} 2 & \text{if } q = 1, \eta \in D_{12}, \text{ or } q = 3, \eta \in D_{r2} \\ 1 & \text{if } q = 2, \eta \in D_{r1} \\ 3 & \text{if } q = 2, \eta \in D_{23} \\ 4 & \text{if } q = 3, \eta \in D_{34} \end{cases}$$

The closed-loop hybrid system resulting from controlling the plant (8)-(9) with the supervisor $\mathcal{H}_s$ and the controllers $\{\mathcal{H}_{c,i}\}_{i=1}^4$ is denoted $\mathcal{H}_{cl} = (C, F, D, G)$ and has state $\chi = (q, \eta)$ with state space $\mathbb{X} := Q \times \mathbb{R}^6$. First, we show that every complete solution to it converges to $\mathcal{A}_4 + \delta_4\mathbb{B}$ in finite time and that renders $\mathcal{A}_4$ asymptotically stable. For this purpose, we use the invariance principle for hybrid systems in [35], for which $\mathcal{H}_{cl}$ has to satisfy the hybrid basic conditions, which is the case. With this design of the hybrid supervisor, and the well-posed hybrid controllers, the proof of Theorem 4.1 is as follows.

6.1. Proof of Theorem 4.1

We show that the hybrid supervisor $\mathcal{H}_s$ constructed above satisfies the properties stated in the claim of Theorem 4.1. Since $\mathcal{H}_{cl}$ satisfies the hybrid basic conditions, following [35, Proposition 6.10], we can conclude every maximal solution to the hybrid system is complete. Now, to show convergence of maximal solutions to $\mathcal{A}_4$, consider the function $V : \mathbb{X} \to \mathbb{R}_{\geq 0}$ defined as $V(\chi) = 4 - q$ for all $\chi \in \mathbb{X}$. During flows, since q remains constant, we have that $\langle \nabla V(\chi), F(\chi) \rangle = 0$ for all $\chi \in C \cap \mathbb{X}$. From initial conditions of the plant in $\mathcal{M}_0 \cap \mathcal{M}_1$ and $q(0,0) = 1$, we have that, at each jump of the supervisor, q is incremented by 1. This implies, for each such jump $V(q^+) - V(q) = -1$. At any jump of the individual controllers, we have $V(q^+) - V(q) = 0$ due to the fact that such jumps do not affect the state q of the supervisor.

Let ϕ be a complete and bounded solution to $\mathcal{H}_{cl}$ with plant initial state in $\mathcal{M}_0 \cap \mathcal{M}_1$ and $q(0,0) = 1$. Applying the invariance principle ([35, Theorem 8.2]), the solution converges to the largest weakly invariant set contained in $C \cap \{\chi \in \mathbb{X} \,:\, V(\chi) = r\,\}$ for some $r \geq 0$. By the properties of V at jumps of the supervisor, if the invariant set has $r > 0$ then the solution remains in a set such that a controller $\mathcal{H}_{c,q}$ with $q < 4$ is applied, which is impossible by the attractivity properties of each individual controllers. Then, ϕ converges to the said largest weakly invariant set with $r = 0$, which corresponds to $q = 4$. By construction of $\mathcal{H}_{c,4}$ we have that the only weakly invariant set is $\mathcal{A}_4$. Stability of $\mathcal{A}_4$ follows from the properties induced by $\mathcal{H}_{c,4}$, while the finite-time stability property follows from the fact that $\mathcal{A}_4 + \delta_4\mathbb{B}$ has $\delta_4 > 0$ and, hence, solutions reach it in finite time. The semiglobal practical asymptotic stability is a consequence of well-posedness of the closed-loop system and the asymptotic stability property of $\mathcal{A}_4$, namely, it follows by an application of [35, Theorem 7.21].

7. 3D Example of spacecraft close proximity mission

7.0.1. Simulation results for individual phases

In this section, we simulate the individual controller design along with Hybrid supervisor discussed in Section 5. To outline these, in Phase I, an LQR feedback controller that compensates for the higher-order nonlinear terms is designed, to which state estimates are fed. In Phase II, we exploit the ideas in [14] (in particular, the change of coordinates), where a proportional-derivative control law that guides the chaser to dock with the target at a desired docking direction ($\alpha = \alpha^*$) and position ($\rho = \rho^*$) is proposed. A logic variable h is introduced to handle the topological obstruction of stabilizing a set on a manifold and designed a logic-based hybrid controller that robustly steers the chaser (either clockwise or counter-clockwise) to reach a point in $\mathcal{X}^{\varepsilon\delta}_{los}$. In Phase-III, a hybrid controller that unites local and "global" controllers is implemented. This controller is designed to induce forward invariance and to satisfy the closing speed constraints for the chaser; in Phase-IV, a LQR controller is designed. Specifically, we use $n = \sqrt{\frac{\mu}{{r_o}^3}}$, $\mu = 3.986 \times 10^{14}\frac{m^3}{s^2}$, $r_o = 7100000m$, $m_c = 500Kg$ and $m_t = 2000Kg$ in the simulations. In the problem definition provided, the chaser starts at a distance of no more than $\rho_{\max} = 10Km$ away from the target. Once docked, the chaser-target has to reach a relocation position with range $\rho(x, y, z) = 20Km$, which is $10Km$ away from the partner spacecraft in worst-case time of $t_f = 12hr$ while maintaining the input constraint $|u|_\infty \leq 0.02m/sec^2$. In Phase I-IV both range ρ and angle α measurements are available and hence we consider that the states $\eta \in \mathbb{R}^6$ can be easily reconstructed as outlined in the beginning of Section 5. A more complete overview of the simulations can be done by considering noise added into the system. A small zero-mean Gaussian residual noise (considering the best performance of a chosen filter) is added to the position and velocity components in every phase[8]. Note that for the combination of the mission parameters and the maximum saturated input, the controller gains for each phase are computed using the trial and error method to satisfy the time constraints. This is a first step solution towards applying hybrid system theory to spacecraft control. Advanced control methods directed towards optimized time and input constraints can be explored for future research directions.

[8]2D simulations: https://github.com/HybridSystemsLab/HybridRendezvousAndDocking; 3D simulations: https://github.com/HybridSystemsLab/HybridRendezvousAndDocking3DOF

Phase I: With these mission parameters, simulations for the entire closed-loop system are performed for the chaser starting from $\eta \in \mathcal{M}_0 \cap \mathcal{M}_1$, which corresponds to various initial conditions in the 10Km radius with a initial velocity $\rho(\dot{x}(0,0), \dot{y}(0,0), \dot{z}(0,0)) \in \left[0, 0.707m/sec\right]$. At this step we consider that the states $\eta \in \mathbb{R}^6$ can be easily reconstructed as outlined in the beginning of Section 5. Hence, two LQR-based controllers are implemented for the $x-y$ and z plane of motion, respectively, with the following choice of weight matrices: $Q_{1a} = 0.015 \times I_{4\times4}$, $R_{1a} = \begin{bmatrix} 20\times10^4 & 0 \\ 0 & 11\times10^4 \end{bmatrix}$, $Q_{1b} = 1.5\times10^{-2}\times I_{2\times2}$, $R_{1b} = 99\times10^3$. Note that, for the combination of the mission parameters and the maximum saturated input $|u|_\infty \leq 0.02m/sec^2$, the gains are computed using the trial and error method to satisfy the maximum time constraint. The trajectories of the chaser during Phase I are shown in Figure 9, and the chaser completes the desired maneuver in this phase in $T_1 \approx 1,7hr$ while maintaining the input constraint $|u|_\infty \leq 0.02m/sec^2$.

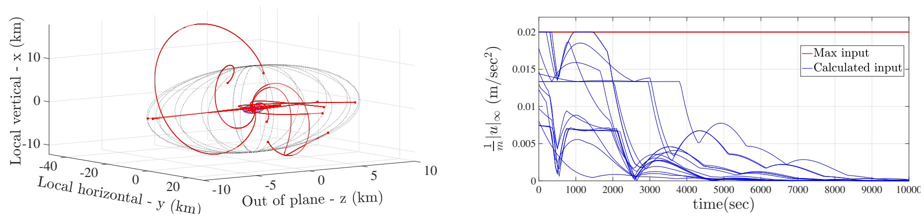

Figure 9: Trajectory of the chaser from various initial conditions and control input during Phase I (corresponds to initial conditions in the 10Km radius and initial velocity $\rho(\dot{x}(0,0), \dot{y}(0,0), \dot{z}(0,0)) \in [0, 0.707m/sec]$).

Phase II: Due to the interesting chaser motion, we also perform multiple simulations when $\mathcal{H}_{c,2}$ is used, for initial position $(x(0,0), y(0,0), z(0,0)) \in D_{12}$, where $D_{12} := \{\eta \in \mathbb{R}^4 : \rho(x,y,z) \in [0, \rho_r]\}$, $\rho_r = 700m$, and initial velocity $\rho(\dot{x}(0,0), \dot{y}(0,0), \dot{z}(0,0)) \in [0, 0.64m/s]$. With $\rho^* = 100m$, $\alpha^* = 179deg$, and $\varrho = 10deg$, the motion of the chaser with both $\ell = 1$ and $\ell = -1$ are shown in Figure 10, which highlights the capabilities conferred by the logic variable in the hybrid controller. For the PD controller κ_{2a}, the gains are chosen as $k_1 = 40$, $k_2 = 0.1$, $k_3 = 25$, $k_4 = 0.047$; instead, for the LQR controller, the weight matrices are $Q = \begin{bmatrix} 138 & 0 \\ 0 & 10 \end{bmatrix}$ and $R = 30\times10^6$. The trajectories of the chaser during Phase II shown in Figure 10 are completed in $T_2 \approx 1hr$, while satisfying the input constraint $|u|_\infty \leq 0.02m/sec^2$. Note that, given the combination of the mission parameters and the maximum saturated input $|u|_\infty \leq 0.02m/sec^2$, the gains are computed using the trial and error method to satisfy the maximum time constraint.

Phase III: We also show the chaser evolution during the approach/closing stage and highlight the specific motion provided by our controller $\mathcal{H}_{c,3}$. Multiple simulations from $(x(0,0), y(0,0), z(0,0)) \in \mathcal{A}_2 + \delta_2\mathbb{B}$, where $\mathcal{A}_2 = \{\eta \in \mathbb{R}^6 : \rho =$

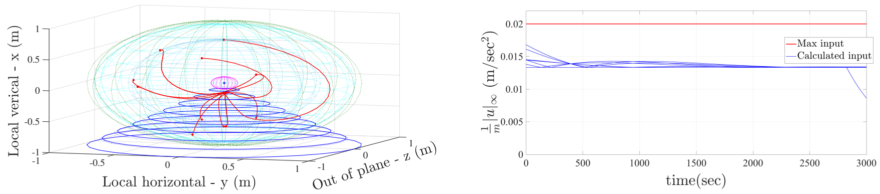

Figure 10: Trajectory of the chaser from various initial conditions and control input during Phase II (corresponds to chasers initial conditions $\rho(x, y, z) \in [0, 700m]$ and initial velocity $\rho(\dot{x}(0,0), \dot{y}(0,0), \dot{z}(0,0)) \in [0, 0.64m/s]$).

$150m, \alpha = \ell\,179deg\}$ and $\delta_2 = 10m$, are presented in the Figure 11. The reference way-point, where the hybrid controller switches between sub controllers is given by $\eta_r = (-25m, \mathbf{0}_{2\times1}m, \mathbf{0}_{3\times1}m/sec)$. For this LQR controller, the weight matrices Q, R and other parameters are chose so that the input constraint $|u|_\infty \leq 0.02m/sec^2$ is satisfied. Once again, for the combination of the mission parameters and the maximum saturated input $|u|_\infty \leq 0.02m/sec^2$, the gains are computed using the trial and error method to satisfy the maximum time constraint. With these gains, the chaser reaches $\delta_3\mathbb{B}$ with $\delta_3 \in [2cm, 8cm]$ for several initial conditions as presented in Figure 11. The closing velocity constraint for the chaser motion during Phase III is shown in Figure 12 and the chaser completes the desired maneuver in $T_3 \approx 0.8hr$.

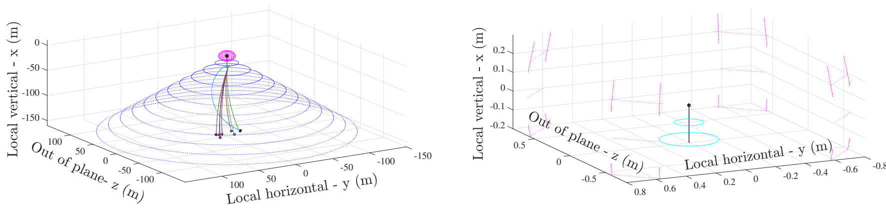

Figure 11: Trajectories of the chaser during Phase III (corresponds to chasers initial conditions close to the docking position $\rho(x, y, z) = 150m$ and docking direction $\alpha = \ell\,179deg$).

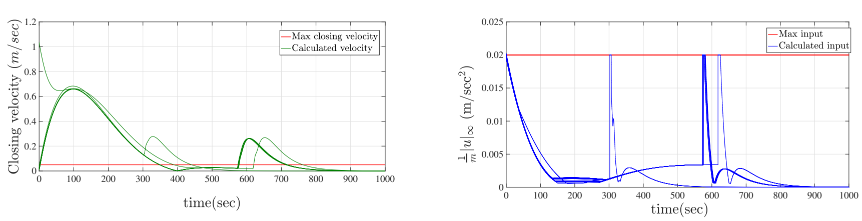

Figure 12: Closing velocity and control input for the chaser during Phase III.

<u>Phase IV</u>: In the last phase, the goal for the chaser-target system is to reach the partner position, $\eta_p = (0km, 20km, 0km, \mathbf{0}_{3\times1}km/sec)$ from various initial

conditions corresponding to docked-phase with $\delta_3 \in [2cm, 8cm]$. In this phase, LQR controller has weight matrices: $Q_a = 6 \times 10^{-1} \times I_{4\times4}$, $R_a = 11 \times 10^4 \times I_{2\times2}$, $Q_b = \begin{bmatrix} 138 & 0 \\ 0 & 10 \end{bmatrix}$ and $R_b = 30 \times 10^6$. Given for the combination of the mission parameters and the maximum saturated input $|u|_\infty \leq 0.02m/sec^2$, the gains are computed using the trial and error method to satisfy the maximum time constraint. The motion of the chaser with mass $m_c + m_t$ is presented in Figure 13 and this maneuver is completed by the chaser-target in $T_4 \approx 1.7hr$ while satisfying the input constraint $|u|_\infty \leq 0.02m/sec^2$.

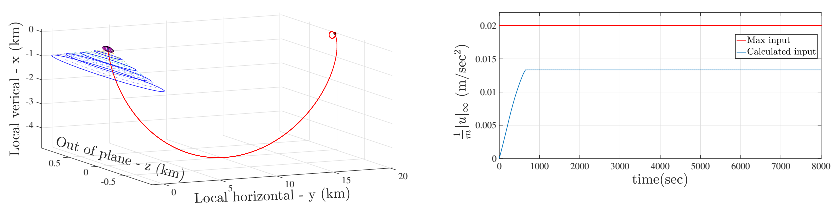

Figure 13: Trajectories of the chaser-target and control input during Phase IV. Initial conditions correspond to the chaser-target's location from $\delta_3 \in [2cm, 8cm]$.

7.0.2. Simulation results from Phase I-IV

Next, complete simulation of chaser and chaser-target dynamics from Phase I-IV is presented in Figures 14 - 16. In this simulation, a hybrid supervisor switches between individual controllers based on the strategy outlined in Section 6. To emulate system and environmental disturbances, in these simulations, the robustness of the controllers for small level of noise is shown, where the chaser reaches the desired neighborhood of the target while maintaining the input constraint $|u|_\infty \leq 0.02m/sec^2$. The total worst case time to reach for the chaser rendezvous, docking and chaser-target rendezvous maneuver is $T_1 + T_2 + T_3 + T_4 \approx 8.88hr < t_f$, which is within specifications.

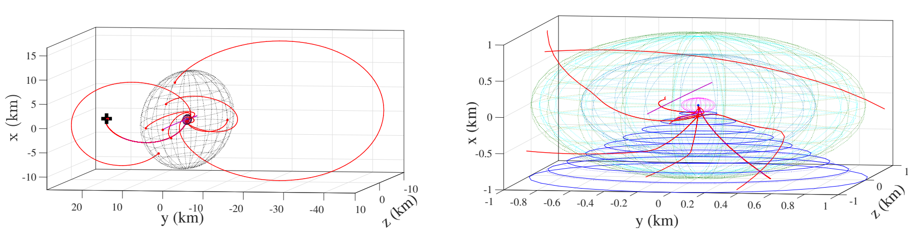

Figure 14: Chaser relative motion for different initial conditions in Phase I, II.

8. Conclusion

For the problem of rendezvous, proximity operations, and docking of an autonomous spacecraft, we characterized the family of individual controllers and

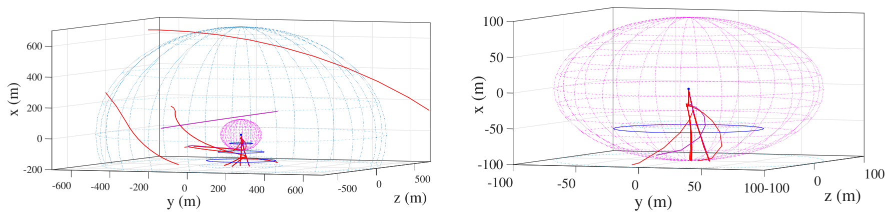

Figure 15: Chaser relative motion for different initial conditions in Phase III.

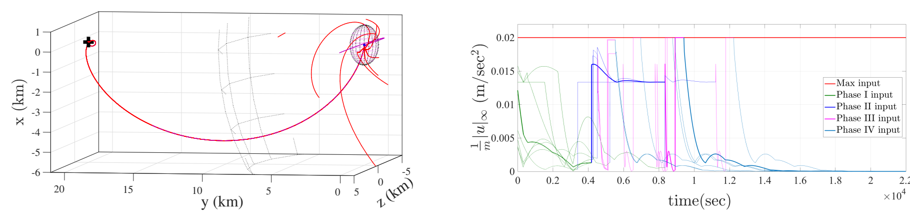

Figure 16: Chaser-target relative motion in Phase I-IV and control input with $m = m_c$ for Phase I-III, $m = m_c + m_t$ for Phase IV.

highlighted the required properties they should induce to the closed-loop system to solve the problem within each phase of operation. In addition, Lyapunov analysis of the individual controllers presented. Particular designs for each phase/controller were proposed for 3D close-proximity space missions. Numerical results validate the approach. This work presents a union of hybrid systems with spacecraft control. In the process of solving a specific close-proximity mission for a spacecraft rendezvous and docking mission, the potential of addressing such complex problem in the hybrid system framework is presented in detail. The bulk of the work in this paper and also corresponding references [6, 7, 26, 41] present a first step solution to show a potential towards a union between two complex fields of research. Specifically, a hybrid supervisory control is successfully proposed and its robustness in the presence of system and environmental disturbances (included as Gaussian noise in simulations) is analyzed in the context of a complex mission that consists of various phases of operation. The controllers proposed in this paper for each phase satisfy the required conditions. While their implementation in real-world platforms is outside the scope of this paper, we foresee that proper discretization and precise detection of the conditions triggered events at which the appropriate controller is selected.

Appendix A. Proof of Theorem 5.1

To show convergence of complete solutions to $\mathcal{A}_2$, consider the Lyapunov function candidate $W \to \mathbb{R}$ given by

$$W(\xi) = W_1(\xi) + W_2(\xi) \qquad \forall \xi \in \mathcal{X} \tag{A.1}$$

where

$$
\begin{aligned}
W_1(\xi) &= \tfrac{1}{2}\begin{bmatrix}\dot{\rho}_e\\ \dot{\alpha}_e\end{bmatrix}^\top \begin{bmatrix}\dot{\rho}_e\\ \dot{\alpha}_e\end{bmatrix} & \forall \xi\in\mathcal{X}\\
W_2(\xi) &= \tfrac{1}{2}\begin{bmatrix}\rho_e\\ \alpha_e\end{bmatrix}^\top \begin{bmatrix}k_2 & 0\\ 0 & k_4\end{bmatrix}\begin{bmatrix}\rho_e\\ \alpha_e\end{bmatrix} & \forall \xi\in\mathcal{X}
\end{aligned}
\tag{A.2}
$$

The Lyapunov function in (A.1) satisfies $W(\xi)=0$ for all $\xi\in\mathcal{A}_2$, $W(\xi)>0$ for all $\xi\notin\mathcal{A}_2$. In addition, for any $c>0$, there exists a $r>0$ such that $W(\xi)>c$ whenever $|\xi|>r$. Thus the set $\Omega_c := \{\xi\in\mathcal{X} : W(\xi)\le c\}$ is compact for every $c>0$. Next, the time derivative of the Lyapunov function candidate W in (A.1) along the flows is given by

$$
\tfrac{d}{dt}W(\xi) \quad = \quad \tfrac{d}{dt}W_1(\xi)+\tfrac{d}{dt}W_2(\xi) \tag{A.3}
$$

since $\ddot{\rho}_e=u_\rho$, $\ddot{\alpha}_e=u_\alpha/\rho$ (see [14, equation 16]), where u_ρ, u_α are defined below (15), it follows:

$$
\tfrac{d}{dt}W(\xi) \quad = \quad -k_1\dot{\rho}_e^2-k_3\dot{\alpha}_e^2. \tag{A.4}
$$

From (A.4), defining for each $\xi\in C_2$

$$
u_C(\xi) := \begin{cases} -k_1\dot{\rho}_e^2-k_3\dot{\alpha}_e^2 & \text{if } \xi\in C_2\\ -\infty & \text{otherwise,}\end{cases} \tag{A.5}
$$

we can see that $\langle\nabla W(\xi), f_2(\xi)\rangle = u_C(\xi)\le 0$.
Next, at jumps, for each $\xi\in D$, the Lyapunov function candidate W in (A.1) changes as follows:

$$
W(g_2(\xi))-W(\xi)=\tfrac{1}{2}k_4(4\ell\alpha\alpha^*)=2\ell\alpha\alpha^* \tag{A.6}
$$

Since $\alpha^*\in(0,\pi]$, $k_4>0$, $\ell\alpha\le-\varrho$, $\varrho\in(0,\pi)$. Therefore, $W(g_2(\xi))-W(\xi)=-2k_4\varrho\alpha^*$. Defining for each $\xi\in D_2\setminus\mathcal{A}_2$

$$
u_D(\xi) := \begin{cases} -2k_4\varrho\alpha^* & \text{if } \xi\in D_2\\ -\infty & \text{otherwise,}\end{cases} \tag{A.7}
$$

we have $W(g_2(\xi))-W(\xi)=u_D(\xi)<0$.

Completeness of maximal solutions: These results show that any solution ϕ to the hybrid system $\mathcal{H}_2$ is bounded and do not blow up in finite time. Also, $g_2(D_2)\subset C_2\cup D_2$ which shows that the every solution ϕ to system $\mathcal{H}_2$ does not jump out of $C_2\cup D_2$. Therefore, from [35, Proposition 2.10], since conditions (b) and (c) therein are not satisfied, we conclude that every maximal solution to the closed-loop system $\mathcal{H}$ is complete.

Application of Invariance Principle for Hybrid Systems: The growth of W along the solutions to $\mathcal{H}_2$ is bounded by $u_C(\xi)$ and $u_D(\xi)$ on $\mathcal{X}$. Because $\mathcal{H}_2$ satisfies the hybrid basic conditions and W in (A.1) is continuous, the invariance principle for hybrid systems in [35, Theorem 8.2] implies that every precompact (complete and bounded) solution to the hybrid system (17) converges to the largest weakly invariant set K contained in

$$W^{-1}(a) \cap \mathcal{X} \cap [\overline{u_C^{-1}(0)} \cup \big(u_D^{-1}(0) \cap g_2(u_D^{-1}(0))\big)] \tag{A.8}$$

for some $a \in \mathbb{R}_{\geq 0}$. By evaluating the dynamics (18) along solutions that remain in (A.8), we have that $\rho_e \equiv \hat{\mathbf{0}} \implies \rho = \rho^*, \alpha_e \equiv \hat{\mathbf{0}} \implies \alpha = \ell\alpha^*$. Then, since the only invariant set is for $a = 0$, (A.8) with $a = 0$ is contained in $\mathcal{A}_2$. Since every maximal solution to $\mathcal{H}_2$ is precompact, then each maximal solution ϕ to $\mathcal{H}_2$ converges to $\mathcal{A}_2$. We conclude that $\mathcal{A}_2$ is globally attractive for the hybrid system $\mathcal{H}_2$. Since the function W in (A.1) is positive-definite relative to $\mathcal{A}_2$ and nonincreasing along the solutions of $\mathcal{H}_2$, then $\mathcal{A}_2$ is stable for $\mathcal{H}_2$.

References

[1] C. Jewison and S. R. Erwin. A spacecraft benchmark problem for hybrid control and estimation. In *2016 IEEE 55th Conference on Decision and Control (CDC)*, pages 3300–3305, 2016.

[2] N. Filipe and P. Tsiotras. Adaptive position and attitude-tracking controller for satellite proximity operations using dual quaternions. *Journal of Guidance, Control, and Dynamics*, 38(4):566–577, 2014.

[3] M. Nazari, E. A. Butcher, T. Yucelen, and A. K. Sanyal. Decentralized consensus control of a rigid-body spacecraft formation with communication delay. *Journal of Guidance, Control, and Dynamics*, 39(4):838–851, 2016.

[4] X. Wang, C. Yu, and Z. Lin. A dual quaternion solution to attitude and position control for rigid-body coordination. *IEEE Transactions on Robotics*, 28(5):1162–1170, 2012.

[5] A. Sanyal, L. Holguin, and S. P. Viswanathan. Guidance and control for spacecraft autonomous chasing and close proximity maneuvers. *IFAC Proceedings Volumes*, 45(13):753–758, 2012.

[6] G. Zucchini, B. P. Malladi, R. G. Sanfelice, and E. Butcher. Robust hybrid supervisory control for a 3-dof spacecraft in close-proximity operations. In *Networked & Autonomous Air & Space Systems*, pages 88–93, 06/2018 2018.

[7] J. R. Crane, C. W. T. Roscoe, B. P. Malladi, G. Zucchini, E. Butcher, R. G. Sanfelice, and I. Hussein. Hybrid control for autonomous spacecraft rendezvous proximity operations and docking. In *Networked & Autonomous Air & Space Systems*, pages 94–99, 06/2018 2018.

[8] P. W. Kelly, R. Bevilacqua, L. Mazal, and R. S. Erwin. Tugsat: removing space debris from geostationary orbits using solar sails. *Journal of Spacecraft and Rockets*, 55(2):437–450, 2018.

[9] P. C. Mark and S. Kamath. Review of active space debris removal methods. *Space Policy*, 47:194–206, 2019.

[10] X. Li, Z. Zhu, and S. Song. Non-cooperative autonomous rendezvous and docking using artificial potentials and sliding mode control. *Proceedings of the Institution of Mechanical Engineers, Part G: Journal of Aerospace Engineering*, 233(4):1171–1184, 2019.

[11] B. P. Malladi, S. Di Cairano, and A. Weiss. Nonlinear model predictive control of coupled rotational-translational spacecraft relative motion. In *2019 American Control Conference (ACC)*, pages 3581–3586. IEEE, 2019.

[12] W. H. Clohessy and R. S. Wiltshire. Terminal guidance system for satellite rendezvous. *Journal of the Aerospace Sciences*, 27(9):653–658, 1960.

[13] G. Hill. Researches in the lunar theory. *American Journal of Mathematics*, 1:5–26, 1878.

[14] C. A. Kluever. Feedback control for spacecraft rendezvous and docking. *Journal of Guidance, Control, and Dynamics*, 22(4):609–611, 1999.

[15] M. Nazari and E. A. Butcher. Fuel efficient periodic gain control strategies for spacecraft relative motion in elliptic chief orbits. *International Journal of Dynamics and Control*, 4:104–122, 2016.

[16] D. Lee, H. Bang, E. A. Butcher, and A. K. Sanyal. Nonlinear output tracking and disturbance rejection for autonomous close range rendezvous and docking of spacecraft. *Transactions of the Japan Society for Aeronautical and Space Sciences*, 57:225–237, 2014.

[17] J. M. Phillips, L. E. Kavraki, and N. Bedrossian. Spacecraft rendezvous and docking with real-time, randomized optimization. In *AIAA Guidance, Navigation, and Control*, 2003.

[18] R. Vazquez, F. Gavilan, and E. F. Camacho. Trajectory planning for spacecraft rendezvous with on/off thrusters. *IFAC Proceedings Volumes*, 44(1):8473–8478, 2011.

[19] A. Weiss, M. Baldwin, R. S. Erwin, and I. Kolmanovsky. Model predictive control for spacecraft rendezvous and docking: Strategies for handling constraints and case studies. *IEEE Transactions on Control Systems Technology*, 23(4):1638–1647, 2015.

[20] E. N. Hartley. A tutorial on model predictive control for spacecraft rendezvous. In *Control Conference (ECC), 2015 European*, pages 1355–1361. IEEE, 2015.

[21] H. Park, S. Di Cairano, and I. Kolmanovsky. Model predictive control for spacecraft rendezvous and docking with a rotating/tumbling platform and for debris avoidance. In *American Control Conference (ACC), 2011*, pages 1922–1927. IEEE, 2011.

[22] S. Di Cairano, H. Park, and I. Kolmanovsky. Model predictive control approach for guidance of spacecraft rendezvous and proximity maneuvering. *International Journal of Robust and Nonlinear Control*, 22(12):1398–1427, 2012.

[23] U. Eren, A. Prach, B. B. Koçer, S. V. Raković, E. Kayacan, and B. Açıkmeşe. Model predictive control in aerospace systems: Current state and opportunities. *Journal of Guidance, Control, and Dynamics*, 2017.

[24] S. S. Farahani, I. Papusha, C. McGhan, and M. R. Murray. Constrained autonomous satellite docking via differential flatness and model predictive control. In *Decision and Control (CDC), 2016 IEEE 55th Conference on*, pages 3306–3311. IEEE, 2016.

[25] N. Chan and S. Mitra. Verifying safety of an autonomous spacecraft rendezvous mission. *ARCH17*, 48:20–32, 2017.

[26] N. Chan and S. Mitra. Verified hybrid lq control for autonomous spacecraft rendezvous. In *Decision and Control (CDC), 2017 IEEE 56th Conference on*, pages 1427–1432. IEEE, 2017.

[27] B. Qi, C. Fan, M. Jiang, and S. Mitra. Dryvr 2.0: A tool for verification and controller synthesis of black-box cyber-physical systems. In *Proceedings of the 21st International Conference on Hybrid Systems: Computation and Control (part of CPS Week)*, pages 269–270, 2018.

[28] B. HomChaudhuri, M. Oishi, M. Shubert, M. Baldwin, and R. S. Erwin. Computing reach-avoid sets for space vehicle docking under continuous thrust. In *Decision and Control (CDC), 2016 IEEE 55th Conference on*, pages 3312–3318. IEEE, 2016.

[29] C. Prieur. Uniting local and global controllers with robustness to vanishing noise. *Math. Control Signals Systems*, 14:143–172, 2001.

[30] D. V. Efimov. Uniting global and local controllers under acting disturbances. *Automatica*, 42:489–495, 2006.

[31] F. Ancona and A. Bressan. Patchy vector fields and asymptotic stabilization. 4:445–471, 1999.

[32] C. Prieur, R. Goebel, and A. R. Teel. Hybrid feedback control and robust stabilization of nonlinear systems. 52(11):2103–2117, November 2007.

[33] R. G. Sanfelice and A. R. Teel. A “throw-and-catch” hybrid control strategy for robust global stabilization of nonlinear systems. In *Proc. 26th American Control Conference*, pages 3470–3475, 2007.

[34] R. Goebel, R. G. Sanfelice, and A.R. Teel. Hybrid dynamical systems. *IEEE Control Systems Magazine*, 29(2):28–93, April 2009.

[35] R. Goebel, R. G. Sanfelice, and A. R. Teel. *Hybrid Dynamical Systems: Modeling, Stability, and Robustness*. Princeton University Press, New Jersey, 2012.

[36] R.G. Sanfelice. *Hybrid Feedback Control*. Princeton University Press, New Jersey, 2021.

[37] K. Alfriend, S. R. Vadali, P. Gurfil, J. How, and L. Breger. *Spacecraft formation flying: dynamics, control and navigation*, volume 2. Butterworth-Heinemann, 2009.

[38] H. Schaub and J. L. Junkins. *Analytical mechanics of space systems*. AIAA, 2003.

[39] B. P. Malladi, R. G. Sanfelice, and E. Butcher. Robust hybrid Kalman filter for a class of nonlinear systems. In *Proceedings of the American Control Conference*, pages 628–633, 2018.

[40] R. G. Sanfelice, M. J. Messina, S. E. Tuna, and A. R. Teel. Robust hybrid controllers for continuous-time systems with applications to obstacle avoidance and regulation to disconnected set of points. In *Proc. 25th American Control Conference*, pages 3352–3357, 2006.

[41] B. Malladi, R. G. Sanfelice, E. Butcher, and J. Wang. Robust hybrid supervisory control for rendezvous and docking of a spacecraft. In *In Proceedings of the Conference on Decision and Control*, pages 3325 – 3330, 2016.